Development 140, 3565-3576 (2013) doi:10.1242/dev.094045

An epigenetic switch is crucial for spermatogonia to exit the undifferentiated state toward a Kit-positive identity

Takayuki Shirakawa[1], Ruken Yaman-Deveci[2], Shin-ichi Tomizawa[1], Yoshito Kamizato[1], Kuniko Nakajima[1], Hidetoshi Sone[1], Yasuyuki Sato[1], Jafar Sharif[2], Akio Yamashita[3], Yuki Takada-Horisawa[2], Shosei Yoshida[4], Kiyoe Ura[5], Masahiro Muto[2], Haruhiko Koseki[2], Toshio Suda[6] and Kazuyuki Ohbo[1,*]

SUMMARY

Epigenetic modifications influence gene expression and chromatin remodeling. In embryonic pluripotent stem cells, these epigenetic modifications have been extensively characterized; by contrast, the epigenetic events of tissue-specific stem cells are poorly understood. Here, we define a new epigenetic shift that is crucial for differentiation of murine spermatogonia toward meiosis. We have exploited a property of incomplete cytokinesis, which causes male germ cells to form aligned chains of characteristic lengths, as they divide and differentiate. These chains revealed the stage of spermatogenesis, so the epigenetic differences of various stages could be characterized. Single, paired and medium chain-length spermatogonia not expressing Kit (a marker of differentiating spermatogonia) showed no expression of Dnmt3a2 and Dnmt3b (two *de novo* DNA methyltransferases); they also lacked the transcriptionally repressive histone modification H3K9me2. By contrast, spermatogonia consisting of ~8-16 chained cells with Kit expression dramatically upregulated Dnmt3a2/3b expression and also displayed increased H3K9me2 modification. To explore the function of these epigenetic changes in spermatogonia *in vivo*, the DNA methylation machinery was destabilized by ectopic Dnmt3b expression or Np95 ablation. Forced Dnmt3b expression induced expression of Kit; whereas ablation of Np95, which is essential for maintaining DNA methylation, interfered with differentiation and viability only after spermatogonia become Kit positive. These data suggest that the epigenetic status of spermatogonia shifts dramatically during the Kit-negative to Kit-positive transition. This shift might serve as a switch that determines whether spermatogonia self-renew or differentiate.

KEY WORDS: Stem cell differentiation, Epigenetics, Germ cells, Kit-negative identity, Kit-positive identity

INTRODUCTION

Stem cells in adults are distinct from progenitor cells in that they can self-renew (Brinster, 2002; Spangrude et al., 1988). Shortly after birth, murine male germ cells acquire stem cell identity; and the mitotic cells that maintain homeostasis through self-renewal during spermatogenesis are known as spermatogonia (Phillips et al., 2010). Spermatogonia are classified as either type A, intermediate or type B. Type A spermatogonia can be subclassified as single (A_s), paired (A_{pr}), aligned ($A_{al\text{-}4}$, $A_{al\text{-}8}$, $A_{al\text{-}16}$ or $A_{al\text{-}32}$) or differentiating (A_1, A_2, A_3 or A_4; supplementary material Fig. S1) (Russell et al., 1999). The A_s theory holds that only A_s cells retain stem cell capacities (de Rooij and Russell, 2000), whereas A_{pr} and A_{al} cells (known as proliferating spermatogonia) are thought to be progenitor cells that can no longer self-renew (de Rooij and Russell, 2000; Huckins, 1971; Oakberg, 1971). Nevertheless, the capacity to self-renew has never been tested in A_{pr}-A_{al} spermatogonia because, until now, the definitive assay was thought to require transplantation of purified A_{pr}-A_{al} cells, and no appropriate purification method is known. An alternative spermatogonia classification method relies on the differential expression of the marker gene Kit: only Kit-negative (Kit^{neg}) spermatogonia show stem cell activity in both neonates and adults (Ohbo et al., 2003; Shinohara et al., 2000). Kit expression commences at the A_1 stage, whereas most A_s, A_{pr} and A_{al} spermatogonia are Kit^{neg} (supplementary material Fig. S1) (de Rooij and Russell, 2000; Yoshinaga et al., 1991). In this article, we distinguish between A_s-A_{al} and $A_{1\text{-}4}$-B spermatogonia by Kit expression.

Other markers are expressed in A_s cells, including GFRα1, Oct4, Plzf, Ngn3 and Nanos2; and their expression profiles assist in understanding stem cell-specific gene networks (supplementary material Fig. S1) (Buageaw et al., 2005; Buaas et al., 2004; Costoya et al., 2004; Ohbo et al., 2003; Sada et al., 2009; Yoshida et al., 2004). All of these markers were detected in subpopulations of A_s, A_{pr} and A_{al} cells, raising questions about the heterogeneity of A_s spermatogonia. In mice, for example, only a small fraction of A_s spermatogonia co-expresses GFRα1 and EGFP in Ngn3-EGFP, whereas the remainder express only one of these genes (Nakagawa et al., 2010; Suzuki et al., 2009). One marker changes its expression pattern during development. Ngn3 is specifically expressed in Kit-negative fraction of neonate spermatogonia, and its expression broadens in adult, overlapping both Kit-negative and Kit-positive spermatogonia (Yoshida et al., 2004; Yoshida et al., 2006; Suzuki et al., 2009). These variable expression patterns in A_s to A_{al} cells could reflect oscillatory expression of lineage-associated genes, differences in cell-cycle status or differential responses to micro-environmental signals. This heterogeneous expression pattern was suggested to reflect a metastable state, in which cells maintain a 'memory of stemness' until they reach a point of no return, and lose stem cell potential (May and Enver, 2001; Graf and Stadtfeld, 2008).

Nuclear architectures have been reported to fix the gene expression program associated with a particular cell fate (Bártová et

[1]Department of Histology and Cell Biology, Yokohama City University School of Medicine, Yokohama 236-0004, Japan. [2]Developmental Genetics group, RIKEN Research Center for Integrative Medical Sciences, Yokohama 230-0045, Japan. [3]Department of Molecular Biology, Yokohama City University School of Medicine,, Yokohama 236-0004, Japan. [4]Division of Germ Cell Biology, National Institute for Basic Biology, Okazaki 444-8585, Japan. [5]Department of Molecular Therapeutics, Osaka University Graduate School of Medicine, Suita 565-0871, Japan. [6]Department of Cell Differentiation, The Sakaguchi Laboratory of Developmental Biology, Keio University School of Medicine, Tokyo 123-8585, Japan.

*Author for correspondence (kohbo@yokohama-cu.ac.jp)

Accepted 27 June 2013

al., 2008; Cremer and Cremer, 2001), so we focused on the chromatin architecture in type A spermatogonia. Undifferentiated spermatogonia typically lack heterochromatin (de Rooij and Russell, 2000), but heterochromatin forms as spermatogonia differentiate (Chiarini-Garcia and Russell, 2002). Heterochromatin formation largely involves accumulation of epigenetic modifications, such as DNA methylation (Grewal and Jia, 2007; Jeltsch, 2006). DNA methylation is mediated primarily by DNA methyltransferase 1 (Dnmt1). In copying the methylation pattern of the original strand in newly replicated DNA, Dnmt1 associates with PCNA and Np95 (Bostick et al., 2007; Sharif et al., 2007). By contrast, if the DNA methylation target is a previously unmethylated site, then *de novo* 5-methylcytosine (5mC) methylation is carried out by two proteins: Dnmt3a and Dnmt3b. In embryonic male germ cells, Dnmt3a2, an isoform of Dnmt3a, and Dnmt3b target specific sites for methylation, including imprinted genes and retrotransposons (Sasaki and Matsui, 2008). Later, Dnmt3a2 and Dnmt3b are again highly expressed in type A spermatogonia (La Salle and Trasler, 2006). Notably, in embryonic stem (ES) cells, Dnmt3a and Dnmt3b are known to interact with Np95, suggesting a link between the two machineries, one that maintains methylation patterns and the other that introduces *de novo* DNA methylation (Meilinger et al., 2009).

Heterochromatin harbors transcriptionally repressive histone tail modifications, such as dimethylated Lys 9 of histone H3 (H3K9me2) (Bártová et al., 2008; Grewal and Jia, 2007). H3K9me2 is mainly associated with facultative heterochromatin, whereas H3K9me3 is observed at constitutive heterochromatin, particularly at pericentromeric heterochromatin (PH). In meiotic spermatogonia, both H3K9me2 and H3K9me3 reportedly are crucial for pairing of homologous chromosomes (Peters et al., 2001; Takada et al., 2011); and although H3K9, H3K27 and H4K20 modifications during the mitotic phase have been characterized histologically (Payne and Braun, 2006), their biological significance with respect to spermatogonial differentiation remains unclear.

To begin to analyze the epigenetic changes occurring in spermatogonia, we took advantage of the fact that germ cells remain connected after division and that their chain length reflects their cell-division history. We exploited this property, and stained the chains for various marker genes, to characterize the epigenetic modifications of type A spermatogonia. Our aim was to extend a marker-based characterization through epigenetic approaches and determine the molecular 'point of no return' for stem cells as they differentiate.

MATERIALS AND METHODS

Mice

The following mice were used: C57BL/6N (Japan SLC), Neurogenin3 (Ngn3)-EGFP (Yoshida et al., 2004), Rosa26mT/mG^{flox} (R26R-tdTomato-EGFP) (Muzumdar et al., 2007), Ngn3-Cre (Yoshida et al., 2004), CAG-loxP-DsRed2-loxP-Flag-Dnmt3b-IRES-EGFP (CAG-DsRed-Flag-Dnmt3b), Oct4-EGFP (Ohbo et al., 2003), Rosa26R-CreER^{T2}:Np95$^{flox/flox}$ (Np95 cKO) and GFRα1-EGFP (Uesaka et al., 2007). The animals were housed in a barrier facility at Yokohama City University. Rosa26mT/mG^{flox} mice were obtained from The Jackson Laboratory (Bar Harbor, Maine, USA). Genotyping PCRs were carried out using tail DNA with the primers listed in supplementary material Table S1.

Flow cytometry

Fluorescence-activated cell sorting (FACS) analysis was performed as described previously (Ohmura et al., 2004). Briefly, encapsulated testes were incubated in PBS supplemented with 1 mg/ml collagenase (Sigma-Aldrich) and 100 units of DNaseI (Invitrogen) for 15 minutes at 37°C with agitation. For Kit staining, suspended cells were incubated at 4°C with Fc-block for 15 minutes and then with APC-anti-Kit antibody (eBiosciences) for 30 minutes. Propidium iodide (2 μg/ml; Sigma-Aldrich) was added, and cells were sorted and analyzed using MoFlo (Beckman-Coluter).

Antibodies

Primary antibodies used for immunohistochemistry were sheep anti-5mC (Capralogics), mouse anti-DNA (AbD Serotec), rabbit anti-Cyp450 (Chemicon), rabbit anti-DDDDK (Abcam), mouse anti-Dnmt3a (IMGENEX), mouse anti-Dnmt3b (IMGENEX), goat anti-Ecad (R&D systems), goat anti-Gata4 (Santa Cruz Biotechnology), rabbit anti-GFP (Millipore), goat anti-GFRα1 (R&D systems), mouse anti-G9a (Perseus Proteomics), mouse anti-GLP (Perseus Proteomics), mouse anti-H3K9me2 (Abcam), rabbit anti-H3K9me2 (Millipore), rat anti-Ki67 (Dako), goat anti-Kit (R&D Systems), rat APC-anti-Kit (eBioscience), mouse anti-Np95 (Abcam), mouse anti-Plzf (Santa Cruz Biotechnology), rabbit anti-Plzf (Santa Cruz Biotechnology), rabbit anti-Sox9 (a gift from Dr Kanai, The University of Tokyo, Tokyo, Japan) and rat anti-Tra98 (a gift from Dr Nishimune, Osaka University, Osaka, Japan) (Tanaka et al., 1997). Secondary antibodies used were goat anti-mouse conjugated to AlexaFluor 488, goat anti-mouse conjugated to AlexaFluor 546, goat anti-rabbit conjugated to AlexaFlour 488, goat anti-rabbit conjugated to AlexaFluor 546, goat anti-rabbit conjugated to AlexaFluor 647, donkey anti-goat conjugated to AlexaFluor 488 (all from Invitrogen) and donkey anti-goat conjugated to biotin (Jackson ImmunoResearch).

Immunohistochemical analysis

Immunohistochemistry of tissue sections was performed as described previously with minor modifications (Ohmura et al., 2004). After sections were incubated with either PBS supplemented with 1% BSA (BSA/PBS) or with MOM blocking reagent (Vector Laboratories), the sections were incubated for either 2 hours at room temperature or overnight at 4°C, with an appropriate primary antibody and then a relevant secondary antibody for 1 hour at room temperature. Nuclear staining was conducted with either TOPRO3 (Invitrogen) or DAPI (Sigma-Aldrich). For 5mC staining and signal quantification, we followed previously reported protocols (Hajkova et al., 2010; Loukinov et al., 2002; Okada et al., 2007; Seki et al., 2005). Briefly, after staining with anti-Plzf or anti-Kit antibody, the specimens were re-fixed with 4% PFA for 30 minutes at room temperature, permeabilized, denatured for 30 minutes in 2 N HCl, and incubated with anti-5mC antibody for 2 hours at room temperature. DAPI served as a nuclear stain. Images were analyzed as reported previously with modifications (Hajkova et al., 2010). The same protocol was applied to the anti-DNA staining. The total intensity of 5mC staining of each nucleus was calculated by NIH Image using the *z*-stack images and normalized to the nuclear area after subtracting the average background pixel intensity. Whole-mount immunohistochemistry was performed as described previously (Ohmura et al., 2004). Briefly, seminiferous tubules were incubated with a relevant primary antibody after blocking, and then reacted with an appropriate secondary antibody. Both section and whole-mouse specimens were covered with Vectashield, and observed by confocal laser microscopy (Carl Zeiss LSM510 or Olympus FV-1000). The TSA Biotin System was used to detect Kit, according to the manufacturer's recommendations (Perkin Elmer).

Bisulfite sequencing

Bisulfite treatment of genomic DNA was performed using EZ DNA Methylation Kit (Zymo Research) as described previously (Hirasawa et al., 2008) with minor modifications. Briefly, DNA extracted from 5×10^4 cells was denatured in 0.3 M NaOH for 20 minutes at 37°C and then treated with 9 M sodium bisulfite. Purified DNA was subjected to desulphonation followed by elution. Bisulfite-treated DNA was then used for PCR, and cloning was performed using pGEM-T Easy Vector Systems (Promega) prior to sequencing. The methylation levels and efficiency of bisulfite conversion were calculated using Quantification Tool for Methylation Analysis (Quma) software (http://quma.cdb.riken.jp). Primer sequences used are listed in supplementary material Table S1.

Reverse transcription PCR (RT-PCR)

Total RNA was isolated from mouse testes using RNeasy Micro Kit (Qiagen) and treated with DNase I (Promega) at 37°C for 20 minutes. First-

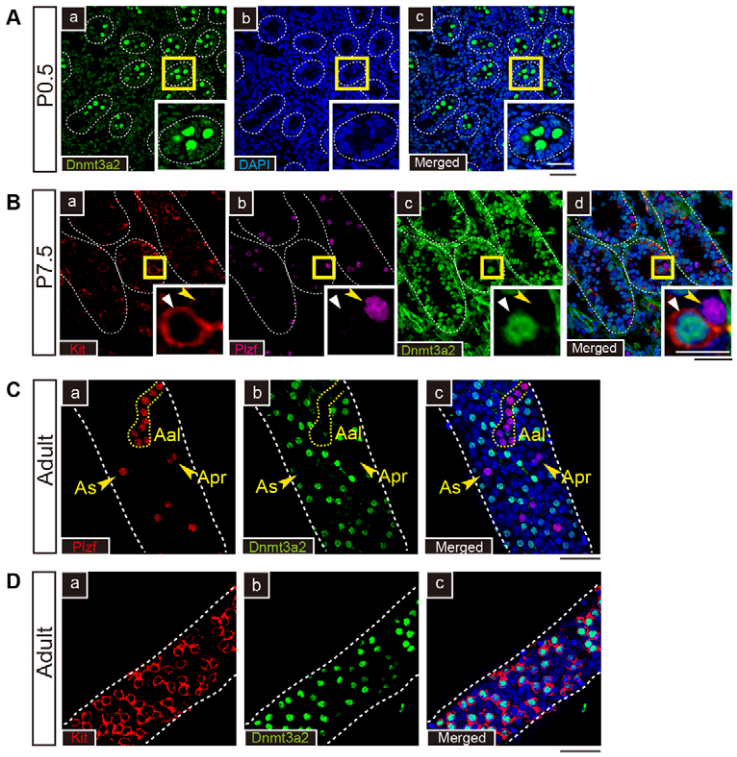

Fig. 1. A_s to A_{al-8} spermatogonia do not express Dnmt3a2. (**A**) (a-c) Immunohistochemical analysis of mouse testis sections. Dnmt3a2 (green) is strongly expressed in P0.5 gonocytes. Scale bars: 50 μm (black); 20 μm (white). Enlargements of the yellow boxed areas are shown in the bottom right-hand corner of each panel. The white dashed lines outline seminiferous tubules. (**B**) (a-d) At P7.5, Dnmt3a2 is expressed only in $Plzf^{neg}/Kit^{pos}$ (white arrowheads), and not in $Plzf^{pos}/Kit^{neg}$ (yellow arrowheads) spermatogonia. Kit, red; Plzf, magenta; Dnmt3a2, green; DAPI, blue. Scale bars: 50 μm (black); 20 μm (white). Enlargements of the yellow boxed areas are shown in the bottom right-hand corner of each panel. The white dashed lines outline seminiferous tubules. (**C**) (a-c) Whole-mount immunohistochemical analysis of Dnmt3a2 (green) and Plzf (red) in adult wild-type mice. Dnmt3a2 is not expressed in spermatogonia from A_s to A_{al} (yellow arrowheads and yellow dashed line, respectively). The white dashed lines outline seminiferous tubules. TOPRO3, blue. Scale bar: 50 μm. (**D**) (a-c) Whole-mount immunohistochemical analysis of Dnmt3a2 (green) and Kit (red) in adult wild-type mice. Kit^{pos} spermatogonia express Dnmt3a2. White dashed lines outline seminiferous tubules. TOPRO3, blue. Scale bar: 50 μm.

strand cDNA was synthesized using Superscript III (Invitrogen). Primers are listed in supplementary material Table S1. The thermal cycling conditions were 94°C for 5 minutes; 40 cycles of 94°C for 30 seconds, 60°C for 30 seconds and 72°C for 30 seconds; and 72°C for 7 minutes.

Quantitative real-time RT-PCR (qPCR)

Dnmt3a1, *Dnmt3a2* and *Hprt* cDNAs were amplified using specific primers (supplementary material Table S1) and cloned with pGEM-T Easy Vector Systems (Promega) to use as templates for determining absolute mRNA levels (supplementary material Fig. S2A,B). Total RNA from sorted cells was isolated and DNase treated as described above. First-strand cDNA synthesis was performed using 100 ng of total RNA, random hexamers and SuperScript III reverse transcriptase. Real-time PCR was carried out using SYBR Premix Ex *Taq*II (Takara) and *Dnmt3a1* and *Dnmt3a2* copy numbers were determined by absolute quantitation. A standard curve was drawn using 10-fold serial dilutions (10 to 10^7 copies) of pGEMT-*Dnmt3a1* and pGEMT-*Dnmt3a2* plasmids. The thermal cycling conditions used were 95°C for 30 seconds, followed by 40 cycles of 95°C for 5 seconds and 60°C for 34 seconds. Experiments were conducted on each subpopulation of cells purified from three independent sorting experiments, with PCRs performed in triplicate.

Western blotting

Western blot analysis of Np95 was performed according to a published method (Sharif et al., 2007). Whole-cell extracts from testis were subjected to 10% sodium dodecyl sulfate PAGE (SDS-PAGE) and proteins were transferred to polyvinylidene difluoride (PVDF) membranes. Membranes were incubated with the Np95 antibody overnight at 4°C, followed by incubation with an appropriate horseradish peroxidase (HRP)-conjugated secondary antibody (Invitrogen) for 1 hour at room temperature. Positive signals were detected and visualized with Chemi-Lumi One reagents (Nacalai tesque, Kyoto, Japan).

RESULTS

A_s to A_{al-8} spermatogonia are largely Dnmt3a2 negative

To characterize the epigenetic machineries in spermatogonia, Dnmt3a2 protein expression was analyzed by immunohistochemistry; in parallel, we analyzed expression of the two markers Plzf and Kit. Triple staining of adult testes revealed that Plzf-positive ($Plzf^{pos}$) but Kit-negative (Kit^{neg}) spermatogonia were negative for Dnmt3a2 (supplementary material Fig. S2E). Conversely, Plzf-negative ($Plzf^{neg}$) but Kit-positive (Kit^{pos}) spermatogonia were positive for Dnmt3a2 (supplementary material Fig. S2E). We noted that Plzf weak-positive and Kit^{pos} spermatogonia also expressed Dnmt3a2 (supplementary material Fig. S2F). Reportedly, differentiating spermatogonia express Kit up to the early spermatocyte stage (Schrans-Stassen et al., 1999; Yoshinaga et al., 1991), so our results indicate that a subpopulation of type A spermatogonia (by definition Kit^{neg}) do not express the DNA methylation protein Dnmt3a2.

As others have shown semi-purified spermatogonia express predominantly Dnmt3a2 (La Salle and Trasler, 2006), our immunohistochemistry probably detected expression of Dnmt3a2, although Dnmt3a1, a longer isoform, can be recognized by the same antibody. To verify that Dnmt3a2 is the isoform predominantly expressed, highly purified spermatogonia from either postnatal day 7.5 (P7.5) Oct4-EGFP (Ohbo et al., 2003) or adult Ngn3-EGFP mice (Yoshida et al., 2004) (supplementary material Fig. S2A-D) were analyzed by qPCR for *Dnmt3a1* and *Dnmt3a2* expression. Confirming expectations, significantly more *Dnmt3a2* was expressed (supplementary material Fig. S2B,D).

Strong Dnmt3a2 expression has been noted in P0.5 gonocytes (Sakai et al., 2004), so expression was tracked in developing newborn mice. Dnmt3a2 was highly expressed in the gonocytes of P0.5 testes (Fig. 1A) and then was rapidly downregulated by P7.5 in $Plzf^{pos}/Kit^{neg}$ spermatogonia, when it became undetectable (Fig. 1B). We and others have shown that, at this stage, when Dnmt3a2 expression is downregulated in $Plzf^{pos}/Kit^{neg}$ spermatogonia, tissue-specific stem cells emerge in testes (McLean et al., 2003, Ohbo et al., 2003). Conversely, Dnmt3a2 is expressed in $Plzf^{neg}/Kit^{pos}$ spermatogonia that have lost stem cell capacity (Fig. 1B) (Ohbo et al., 2003).

To track the cell division history of the $Kit^{neg}/Dnmt3a2^{pos}$ spermatogonia, we examined expression profiles of various

Table 1. Dnmt3a2^{pos} chain distribution in A_s-A_{al-8} spermatogonia

	A_s	A_{pr}	A_{al-4}	A_{al-8}
Dnmt3a2^{pos}/GFRα1^{pos}	0/267	0/151	0/55	0/4
Dnmt3a2^{pos}/Plzf^{pos}	0/166	0/131	0/78	0/81
Dnmt3a2^{pos}/Ngn3-EGFP^{pos}	0/36	0/31	0/56	2 /47
Total	0/469	0/313	0/189	2 /132

The number of Dnmt3a2^{pos} chains that are GFRα1^{pos}, Plzf^{pos} or Ngn3-EGFP^{pos} among A_s, A_{pr}, A_{al-4} and A_{al-8} spermatogonia counted in the whole-mount immunohistochemistry images in Fig. 1.

Table 2. Dnmt3b^{pos} chain distribution in A_s-A_{al-8} spermatogonia

	A_s	A_{pr}	A_{al-4}	A_{al-8}
Dnmt3b^{pos}/GFRα1^{pos}	0/280	0/133	0/89	0/6
Dnmt3b^{pos}/Plzf^{pos}	0/219	0/165	0/92	0/95
Dnmt3b^{pos}/Ngn3-EGFP^{pos}	0/23	0/46	0/72	0/67
Total	0/522	0/344	0/253	0/168

The number of Dnmt3b^{pos} chains that are GFRα1^{pos}, Plzf^{pos} or Ngn3-EGFP^{pos} among A_s, A_{pr}, A_{al-4} and A_{al-8} spermatogonia counted in the whole-mount immunohistochemistry images in Fig. 2.

spermatogonial markers. Immunohistochemistry of whole-mount testes tracked co-expression of Dnmt3a2 with three markers expected on A_s, A_{pr} and A_{al} cells (i.e. GFRα1, Plzf and an EGFP reporter driven by the Ngn3 regulatory sequence Ngn3-EGFP), and one marker expected on A_1 spermatogonia, Kit (Fig. 1C,D; supplementary material Fig. S2G). Double-staining of adult testes with Plzf and Dnmt3a2 antibodies revealed that not only A_s but also A_{pr}, A_{al-4} and A_{al-8} spermatogonia lacked Dnmt3a2 expression (Fig. 1C, Table 1). This finding was confirmed in GFRα1^{pos} (Table 1; supplementary material Fig. S2Ga-c) and Ngn3-EGFP^{pos} spermatogonia (Table 1; supplementary material Fig. S2Gd-f), although the latter showed weak Dnmt3a2 staining in two out of 47 chains for A_{al-8} spermatogonia (Table 1; supplementary material Fig. S2H). Conversely, the Dnmt3a2 expression pattern paralleled that of Kit, suggesting Dnmt3a2 expression is initiated in A_1 differentiating spermatogonia (Fig. 1D; supplementary material Fig. S2I). A small population of chains of four spermatogonia existing at stages VIII-X is Kit positive (A_1 spermatogonia) and express Dnmt3a2 (supplementary material Fig. S2J). Thus, the markers we tested suggested that A_s, A_{pr} and A_{al} spermatogonia were Dnmt3a2 negative. Taken together, these data suggest that by the end of the first postnatal week, Dnmt3a2 is downregulated in spermatogonia and only upregulated again when spermatogonia begin to express Kit and differentiate.

Spermatogonia in neonatal and adult mice from A_s to A_{al-8} are also Dnmt3b-negative

In contrast to Dnmt3a2, Dnmt3b was barely detectable in P0.5 gonocytes (Fig. 2A), but by P7.5, Dnmt3b appeared in Plzf^{neg}/Kit^{pos} spermatogonia but not in Plzf^{pos}/Kit^{neg} spermatogonia (Fig. 2B). Double staining for Plzf and Dnmt3b of adult testes revealed that from stages A_s to A_{al-8}, spermatogonia do not express Dnmt3b (Fig. 2C). Similar findings were observed in GFRα1^{pos} and Ngn3-EGFP^{pos} spermatogonia (supplementary material Fig. S2K), with Dnmt3b expression positively correlated with Kit expression (Fig. 2D). In a similar manner to Dnmt3a2, we noted a small number of chains of four spermatogonia existing at stages VIII-X is Kit positive (A_1 spermatogonia), and they expressed Dnmt3b (supplementary material Fig. S2L). The Dnmt3b expression patterns in adult spermatogonia are summarized in Table 2: collectively, spermatogonia from A_s to A_{al-4} and the majority of A_{al-8} cells lacked *de novo* Dnmts (Tables 1, 2); and in both neonates and adults, type A spermatogonia that express Dnmt3a2 and Dnmt3b also express Kit.

DNA methylation status of Kit^{neg} and Kit^{pos} spermatogonia

How does the expression of these DNA methylating proteins affect DNA methylation in spermatogonia? To evaluate global methylation of Plzf^{pos}/Kit^{neg} and Plzf^{neg}/Kit^{pos} spermatogonia,

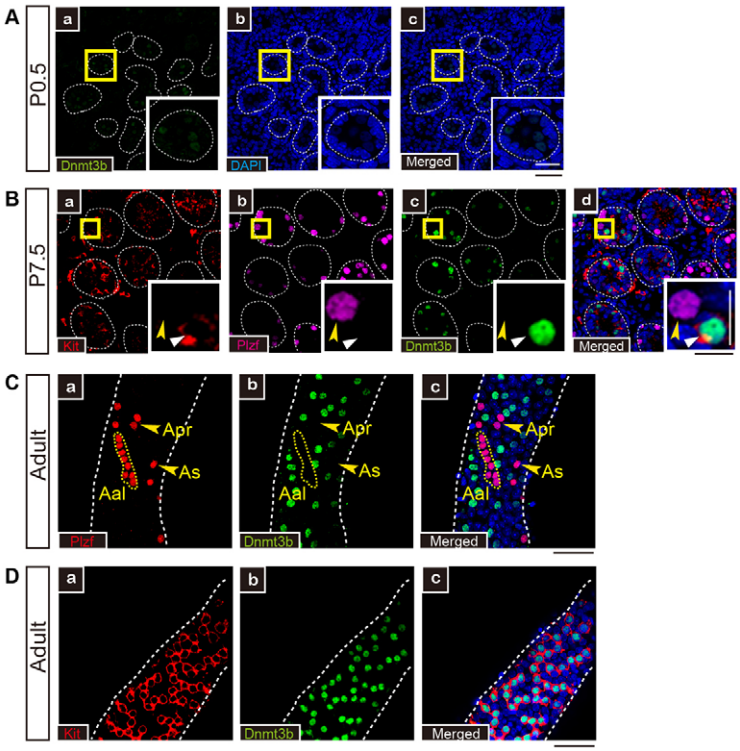

Fig. 2. A_s to A_{al-8} spermatogonia do not express Dnmt3b. (**A**) (a-c) Immunohistochemical analysis of mouse testis sections for Dnmt3b. Dnmt3b (green) is barely detectable in P0.5 gonocytes. Scale bars: 50 μm (black); 20 μm (white). Enlargements of the yellow boxed areas are shown in the bottom right-hand corner of each panel. The white dashed lines outline seminiferous tubules. (**B**) (a-d) At P7.5, Dnmt3b is expressed only in Plzf^{neg}/Kit^{pos} (white arrowheads) but not in Plzf^{pos}/Kit^{neg} (yellow arrowheads) spermatogonia. Kit, red; Plzf, magenta; Dnmt3b, green; DAPI, blue. Scale bars: 50 μm (black); 20 μm (white). Enlargements of the yellow boxed areas are shown in the bottom right-hand corner of each panel. The white dashed lines outline seminiferous tubules. (**C**) (a-c) Whole-mount immunohistochemical analysis of Dnmt3b (green) and Plzf (red) in adult wild-type mice. Dnmt3b is not expressed in spermatogonia from A_s to A_{al} (yellow arrowheads and yellow dashed line, respectively). White dashed lines outline seminiferous tubules. TOPRO3, blue. Scale bars: 50 μm. (**D**) (a-c) Whole-mount immunohistochemical analysis of Dnmt3b (green) and Kit (red) in adult wild-type mice. Kit^{pos} spermatogonia express Dnmt3b. White dashed lines outline seminiferous tubules. TOPRO3, blue. Scale bar: 50 μm.

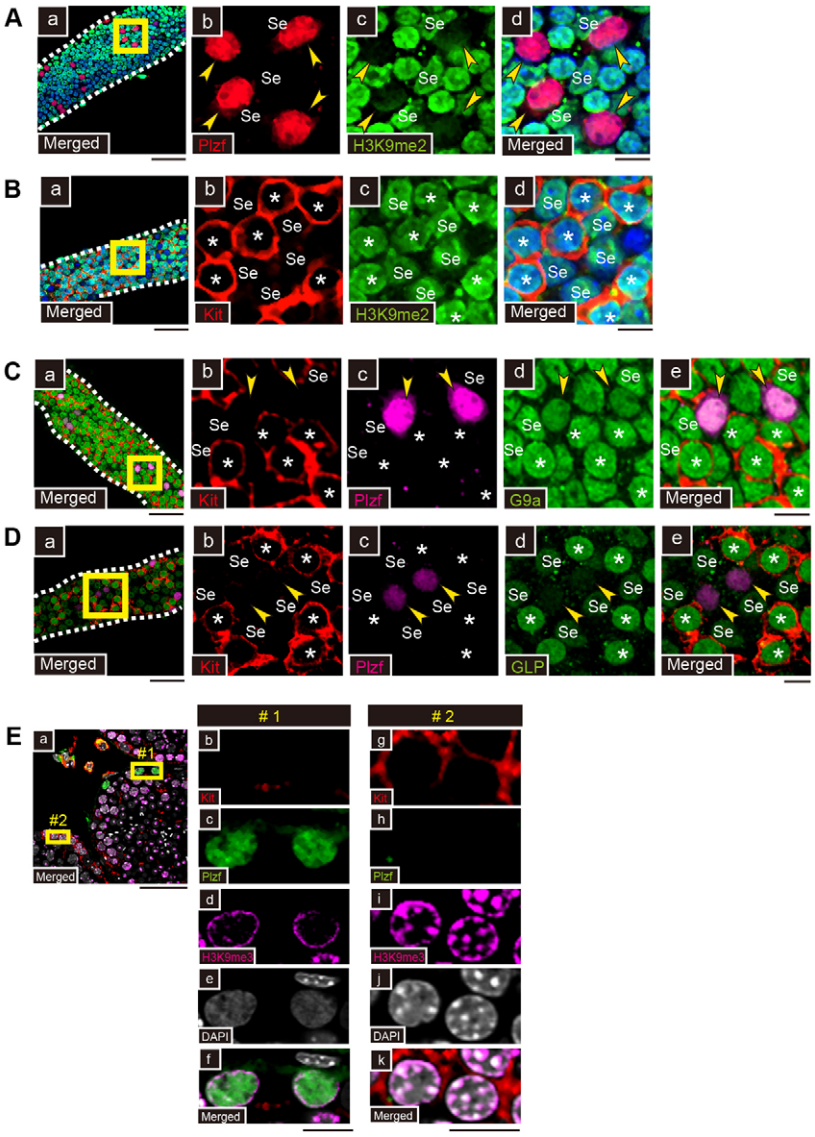

Fig. 3. Patterns of repressive H3K9 marks are altered at the Kit^{neg} to Kit^{pos} transition in spermatogonia. (**A**) Whole-mount immunohistochemical images of a seminiferous tubule showing that spermatogonia expressing Plzf (red) lack H3K9me2 modification (green, yellow arrowheads). The boxed area (a) is enlarged in b-d. Dashed lines indicate seminiferous tubules. Se, Sertoli cells. DAPI, blue. Sertoli cells are identified by the pattern of DAPI staining. Scale bars: 50 μm in a; 10 μm in b-d. (**B**) Spermatogonia expressing Kit (red, asterisks) show H3K9me2 modification (green). The boxed area (a) is enlarged in b-d. Dashed lines indicate seminiferous tubules. Se, Sertoli cells. DAPI, blue. Sertoli cells are identified by DAPI staining. Scale bars: 50 μm in a; 10 μm in b-d. (**C**) G9a protein expression in spermatogonia. Plzf^{pos}/Kit^{neg} (yellow arrowheads) and Plzf^{neg}/Kit^{pos} spermatogonia (asterisks) express G9a (green) at similar levels. Se, Sertoli cells. The boxed area in a is enlarged in b-e. Dashed lines outline seminiferous tubules. Scale bars: 50 μm in a; 10 μm in b-e. (**D**) GLP expression in spermatogonia. Plzf^{pos}/Kit^{neg} spermatogonia (yellow arrowheads) weakly express GLP (green), whereas Plzf^{neg}/Kit^{pos} spermatogonia (asterisks) highly express GLP. Boxed area in a is enlarged in b-e. Dashed lines indicate seminiferous tubules. Se, Sertoli cells. Scale bars: 50 μm in a; 10 μm in b-e. (**E**) H3K9me3 localization changes at the Kit^{neg} to Kit^{pos} transition in adult wild-type mice. H3K9me3 is enriched at the periphery of nuclei in Plzf^{pos}/Kit^{neg} spermatogonia (box 1 in a; enlargements are shown in b-f). In Plzf^{neg}/Kit^{pos} spermatogonia, H3K9me3 specifically accumulates in DAPI-dense areas in addition to the periphery, and represents the PH regions (box 2 in a with enlargements shown in g-k). Kit, red; H3K9me3, magenta; Plzf, green; DAPI, gray. Scale bars: 50 μm in a; 10 μm in b-k.

cytosine 5 methylation was tracked with a previously characterized sheep-anti-5mC antibody, in 3D confocal immunohistochemical analysis (Loukinov et al., 2002) (supplementary material Fig. S3A). The results of this assay implied that the DNA was less methylated in Plzf^{pos}/Kit^{neg} spermatogonia (supplementary material Fig. S3A). To quantitate the difference in signal strength, we summed the anti-5mC signal from the *z*-section images spanning the nucleus (NIH Image). Twelve cells were analyzed from each cell type (i.e. Plzf^{pos}/Kit^{neg} and Plzf^{neg}/Kit^{pos} spermatogonia, and control Sertoli cells). Moreover, to confirm that the antibody indeed had access to the methylated DNA, the chromosomes were also stained with an anti-DNA antibody under denaturing conditions (supplementary material Fig. S3C,D). This careful analysis revealed that although Plzf^{neg}/Kit^{pos} spermatogonia and Sertoli cells stained equivalently, Plzf^{pos}/Kit^{neg} spermatogonia showed comparatively ~2- to 3-fold weaker staining for 5mC (supplementary material Fig. S3B). These data suggest that when spermatogonia undergo the Kit^{neg} to Kit^{pos} transition, the signal strength of 5mC increases with level of Dnmt expression. A future analysis could characterize this genome-wide methylation change at the sequence level.

To examine cytosine methylation of genes known to be crucial for spermatogonial differentiation, FACS-purified GFRα1-EGFP^{pos}/Kit^{neg} and Ngn3-EGFP^{pos}/Kit^{pos} spermatogonia from adults were analyzed by bisulfite sequencing. Methylation was assessed in the promoters and enhancer regions of two spermatogonial marker genes: *plzf* and *kit*; these might be methylated distinctly as Plzf, a repressor protein, and Kit have inverse expression patterns (Filipponi et al., 2007). The *kit* enhancer region includes two putative Plzf-binding sites (Filipponi et al., 2007; Spinello et al., 2009), but these sites were similarly methylated in GFRα1-EGFP^{pos}/Kit^{neg} and Ngn3-EGFP^{pos}/Kit^{pos} spermatogonia (supplementary material Fig. S3E). However, methylation of the *plzf* regulatory region was higher in Ngn3-EGFP^{pos}/Kit^{pos} spermatogonia than in GFRα1-EGFP^{pos}/Kit^{neg} spermatogonia (91.3% and 61.8%, respectively; supplementary material Fig. S3F), suggesting the *plzf* promoter is less likely to be permissive for transcription factors to bind in the Kit^{pos} cells. Similarly, methylation of the enhancer of *oct4* (a marker gene for undifferentiated cells) (Pesce et al., 1998) was higher in Ngn3-EGFP^{pos}/Kit^{pos} spermatogonia than in GFRα1-EGFP^{pos}/Kit^{neg} spermatogonia (52.3% and 16.0%, respectively; supplementary material Fig. S3G). These results suggest that DNA methylation might directly or indirectly regulate some of the genes guiding spermatogonial differentiation. In the future, whole-genome

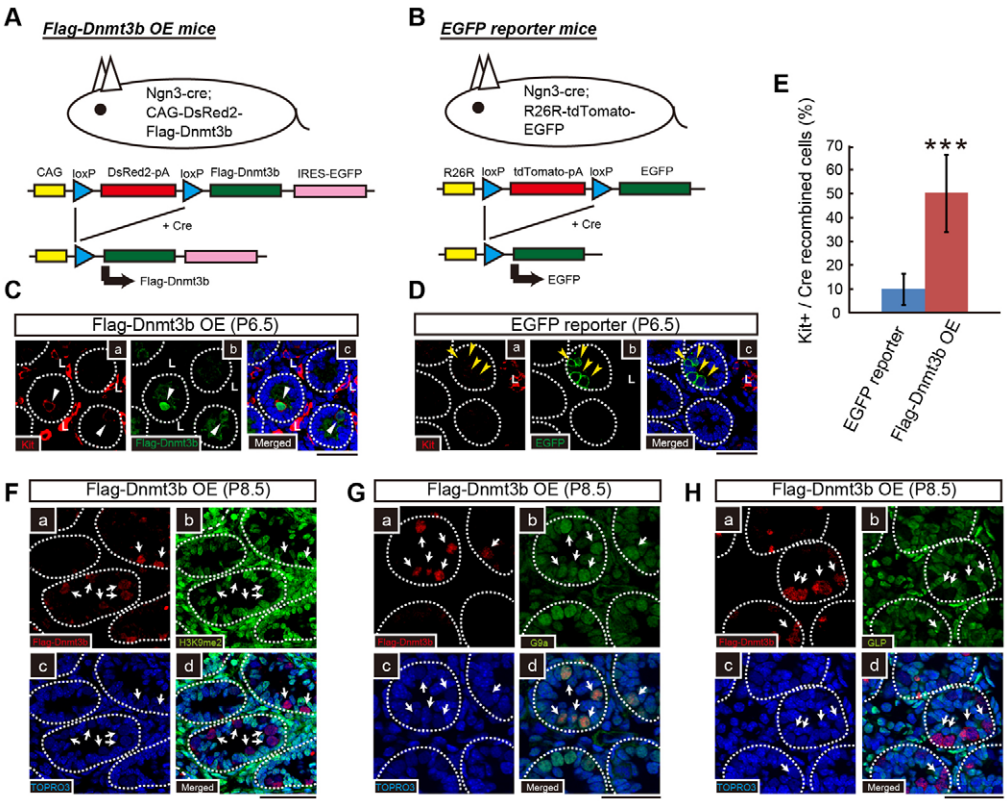

Fig. 4. Dnmt3b expression in Plzf^{pos}/Kit^{neg} spermatogonia induces Kit expression. (**A**) A conditionally induced Dnmt3b expression system in Plzf^{pos}/Kit^{neg} spermatogonia. Ngn3-cre mice were crossed with CAG-DsRed2-Flag-Dnmt3b mice, which express Flag-Dnmt3b following Cre-mediated removal of the poly-A-containing DSRed2 fragment (Flag-Dnmt3b OE mice). (**B**) A control reporter transgenic line. Ngn3-cre mice were crossed with R26R-tdTomato-EGFP reporter mice expressing EGFP after Cre-mediated removal of the tdTomato-pA sequence (EGFP reporter mice). (**C**) Conditional expression of Dnmt3b induces Kit expression. Kit^{pos} spermatogonia are frequently observed in Flag-Dnmt3b^{pos} spermatogonia (white arrowheads; a-c). (**D**) Ngn3-driven Cre expression observed by EGFP reporter at the neonatal stage is largely restricted to Kit^{neg} spermatogonia. EGFP^{pos} spermatogonia were mostly Kit^{neg} (yellow arrowheads; a-c). (**E**) Proportion of Kit^{pos} cells among EGFP^{pos} (control) and Dnmt3b-expressing spermatogonia (Flag-Dnmt3b OE mice). Counts of immunohistochemically double-stained cells revealed the ratio of Kit^{pos} to recombined cells (EGFP reporter, *n*=30-48 per mouse; Flag-Dnmt3b OE, *n*=30-53 per mouse; three mice each). *P* values were derived from *t*-tests; ***P<0.001. Values are presented as mean±s.d. (**F**) (a-d) Flag-Dnmt3b^{pos} spermatogonia (red, white arrows) do not show H3K9me2 signals (green). (**G**) (a-d) Flag-Dnmt3b^{pos} spermatogonia (red, white arrows) express G9a (green). (**H**) (a-d) Flag-Dnmt3b^{pos} spermatogonia (red, white arrows) do not express GLP (green). White dashed lines outline seminiferous tubules. TOPRO3, blue. Scale bars: 50 μm.

bisulfite sequencing should be able to clarify the picture of methylation changes in differentiating spermatogonia.

H3K9me2 and H3K9me3 modification patterns are altered differently at the Kit^{neg} to Kit^{pos} transition in spermatogonia

H3K9 modifications are directly linked to large-scale organizations of chromosomal territories and chromocenter formation, which may fix a gene expression program associated with a particular cell fate (Bártová et al., 2008; Cremer and Cremer, 2001). To determine when H3K9me2 modification increases, whole-mount adult testes were probed immunohistochemically with the markers, Plzf, GFRα1, Ngn3-EGFP and Kit (Fig. 3A,B; supplementary material Fig. S4A). This analysis showed that, regardless of the spermatogonial marker used, A_s, A_{pr} and A_{al} spermatogonia showed only weak levels of H3K9me2 modification compared with neighboring cells (Fig. 3A; supplementary material Fig. S4A). Double staining with anti-Kit and anti-H3K9me2 antibodies showed that all Kit^{pos} spermatogonia exhibited strong H3K9me2 signals (Fig. 3B).

The H3K9me2 methylation is primarily catalyzed by two enzymes, G9a and GLP. So to confirm the results with the double staining of anti-Kit and anti-H3K9me2 antibodies, G9a and GLP expression was tracked in Kit^{neg} and Kit^{pos} spermatogonia. This experiment revealed that although G9a was ubiquitously expressed (Fig. 3C), GLP protein expression was stronger in Plzf^{neg}/Kit^{pos} spermatogonia compared with Kit^{neg} spermatogonia (Fig. 3D).

Although G9a knockout mice manifest male germ cell abnormalities at the meiotic pachytene stage (Tachibana et al., 2007), our result suggests that H3K9me2 modification is already established in spermatogonia during the mitotic stage, in particular at the Kit^{neg} to Kit^{pos} transition. These data, then, suggest that H3K9me2 methylation rises simultaneously with Dnmt3a2 and Dnmt3b expression, and the enhancement of 5mC signals (supplementary material Fig. S4B).

By contrast, another repressive histone modification, H3K9me3, showed a distinct localization pattern: it is partitioned in a ring-like pattern, without a densely stained DAPI area (consistent with a previous report by Payne and Braun, 2006). This pattern was detected only in Plzf^{pos}/Kit^{neg} spermatogonia (Fig. 3Eb-f). Meanwhile, Plzf^{neg}/Kit^{pos} spermatogonia contained DAPI-dense areas that accumulated H3K9me3, a signal characteristic of PH regions (Fig. 3Eg-k). These data indicate that global levels of H3K9me2 increase

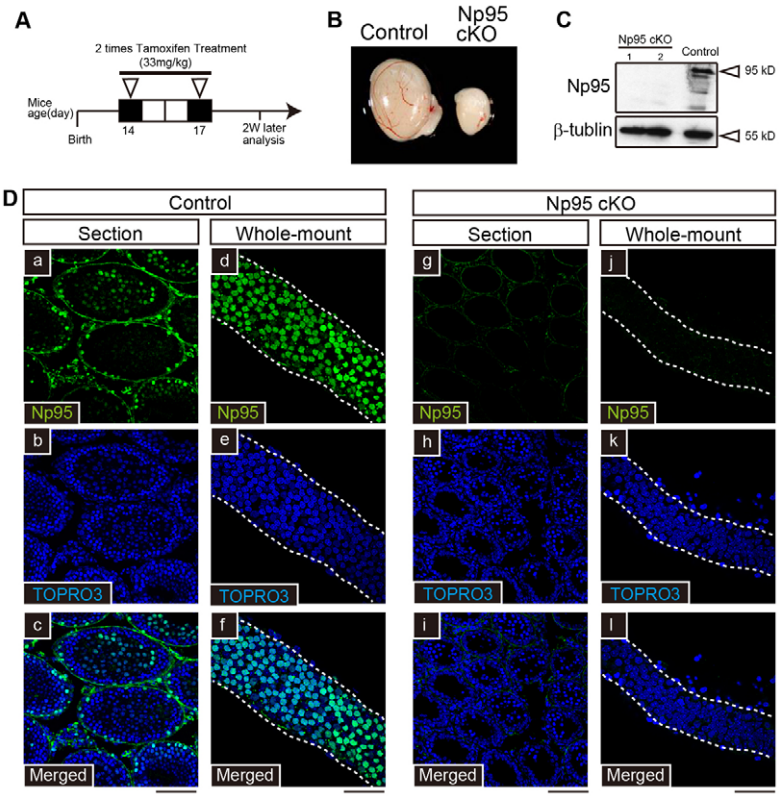

Fig. 5. Generation of tamoxifen-induced *Np95* cKO mice. (**A**) The time course of tamoxifen administration and analysis of *Np95* cKO mice. Tamoxifen was injected intraperitoneally (33 mg/kg) at day 14 and 17. Animals were analyzed 2 weeks after the first injection. (**B**) Np95 cKO mouse testes (right) were significantly smaller than those of littermate controls (left) at 4 weeks of age. (**C**) Western analysis of Np95 in two Np95 cKO mice (lanes 1 and 2) and a littermate control; β-tubulin was the internal control. (**D**) Immunohistochemical analysis of Np95 in seminiferous tubules of Np95 cKO and control mice. Immunohistochemistry on tissue sections from littermate controls (a-c) and Np95 cKO mice (g-i). Whole-mount immunohistochemical analysis of littermate controls (d-f) and Np95 cKO mice (j-l). Dashed lines outline seminiferous tubules. Np95, green; TOPRO3, blue. Scale bars: 100 μm in a-c,g-i; 50 μm in d-f,j-l.

during the Kit^{neg} to Kit^{pos} transition; and this change could mainly result from the activity of GLP rather than G9a. The appearance of the nuclear DAPI foci associated with changes in H3K9me3 localization suggests that, in interphase nuclei at the Kit^{neg} to Kit^{pos} transition, chromosomal organization might also significantly change.

Ectopic Dnmt3b expression in Kit^{neg} spermatogonia induces Kit expression but no change in H3K9me2 modification

To assess the influence of Dnmt3 expression *in vivo*, $Plzf^{pos}/Kit^{neg}$ spermatogonia were manipulated to conditionally express a Flag-tagged Dnmt3b. To achieve this, Ngn3-cre:CAG-DsRed2-Flag-Dnmt3b mice were induced to undergo a Cre-mediated recombination *in vivo* (Fig. 4A). Flag-Dnmt3b expression should be triggered only in cells expressing Ngn3 in neonates, which includes $Oct4^{pos}/Kit^{neg}$ spermatogonia in newborn mouse testes (Yoshida et al., 2004). To confirm Cre-driven recombination, Ngn3-cre mice were crossed with R26R-tdTomato-EGFP mice and analyzed at P6.5 (Fig. 4B); EGFP/Plzf double staining confirmed that $EGFP^{pos}$ spermatogonia expressed Plzf (supplementary material Fig. S5Aa,b), and only a small number of them expressed Kit in P6.5 testes (supplementary material Fig. S5Ac,d), strongly suggesting recombination occurred predominantly in $Plzf^{pos}/Kit^{neg}$ spermatogonia. We also performed cross-sectional analysis of Ngn3-EGFP mouse testis in which the same Ngn3 regulatory sequence drives EGFP. This analysis also revealed that most of the Ngn3-$EGFP^{pos}$ spermatogonia from P6.5 mice were Kit^{neg} (supplementary material Fig. S5Ae,f).

To test whether Dnmt3b expression at P6.5 induced Kit expression, mice overexpressing Flag-tagged Dnmt3b were analyzed by immunohistochemistry, revealing that Flag-positive spermatogonia tended to co-express Kit in P6.5 testes (Fig. 4C). Cre and Flag-Dnmt3b expression was confirmed by RT-PCR (supplementary material Fig. S5B). Moreover, tissue sections showed that almost 50% of Flag-$Dnmt3b^{pos}$ spermatogonia were also Kit^{pos} (Fig. 4C,E). By contrast, in EGFP reporter control mice, ~10% of $EGFP^{pos}$ spermatogonia were Kit^{pos} (Fig. 4D,E). To exclude the possibility that these differences in frequency were due to differences in promoter strength or to distance between loxP sites, we assessed the recombination frequency of both transgenes and found the differences were negligible (see supplementary material Fig. S5C). Interestingly, Flag-$Dnmt3b^{pos}$ spermatogonia showed weak signals of H3K9me2, even in P8.5 testes (Fig. 4F); and subsequent analysis of G9a and GLP expression showed that GLP was not upregulated by the ectopic expression of Dnmt3b (Fig. 4G,H). It is also noteworthy that Flag-Dnmt3b-positive cells do not appear to undergo meiosis (data not shown), possibly owing to a disturbance in the physiological dynamic demethylation and methylation wave that occurs during meiosis (Loukinov et al., 2002).

Interference with Np95-mediated DNA methylation in spermatogonia perturbs differentiation potential

Genomic methylation patterns are maintained in dividing cells, in part, because Np95 at DNA replication forks recruits Dnmt1 (Bostick et al., 2007; Sharif et al., 2007). In addition, Np95 binds H3K9me2/3 and associates with PH regions, thereby linking DNA methylation to heterochromatin formation (Nady et al., 2011; Papait et al., 2007; Papait et al., 2008; Rottach et al., 2010). To assess how DNA methylation-linked heterochromatin formation influences spermatogonial stem cell differentiation, we established a tamoxifen-inducible, conditional knockout (cKO) of Np95 (supplementary material Fig. S6A). Tamoxifen-induced knockout of Np95 was confirmed by western blotting, immunohistochemistry and genomic PCR (Fig. 5C,D; supplementary material Fig. S6B).

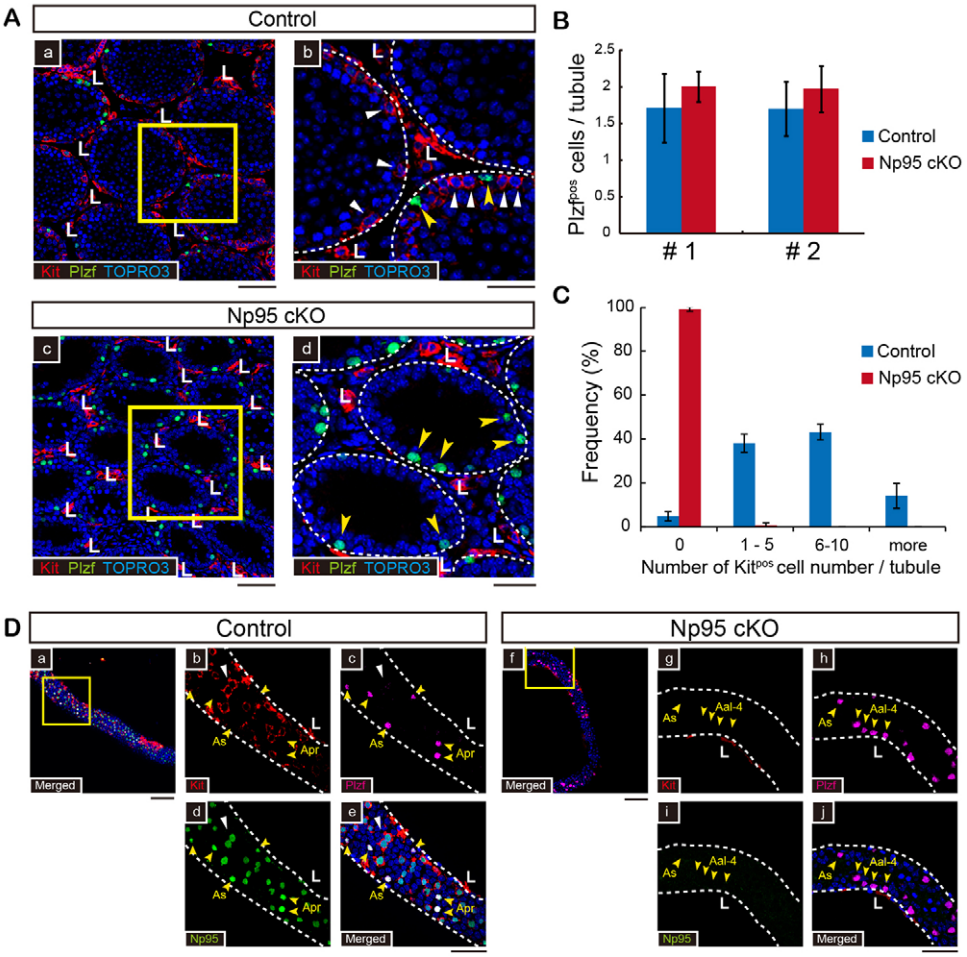

Fig. 6. Spermatogonial differentiation is blocked at the Kit^{neg} to Kit^{pos} transition in Np95 cKO mice. (**A**) Immunohistochemical analysis of sections showing Kit (red) and Plzf (green) expression in control (a,b) and Np95 cKO (c,d) mouse testes. Plzf^{pos}/Kit^{neg} spermatogonia (yellow arrowheads) are found in Np95 cKO and control mice, whereas Plzf^{neg}/Kit^{pos} spermatogonia (white arrowheads) are barely detected in Np95 cKO mice. Kit expression in Leydig cells (L) is similar in control and Np95 cKO mice. TOPRO3, blue. Scale bars: 100 μm in a,c; 50 μm in b,d. (**B**) The number of Plzf^{pos}/Kit^{neg} spermatogonia remained unchanged in Np95-depleted testes. Cell counts using immunohistochemistry images from two independent experiments (control #1, *n*=270; control #2, *n*=255; Np95 #1, *n*=345; Np95 #2, *n*=310) are shown. Values are presented as mean±s.d. (**C**) The number of Kit^{pos} spermatogonia per seminiferous tubule. In contrast to controls (*n*=128), most Np95-cKO spermatogonia (*n*=60) do not express Kit. (**D**) Whole-mount immunohistochemistry of Kit (red), Plzf (magenta) and Np95 (green) in control (a-e) or Np95 cKO (f-j) mouse seminiferous tubules. In Np95 cKO mice (f-j), Plzf^{pos}/Kit^{neg} spermatogonia (yellow arrowheads), including A_s, A_{pr}, A_{al-4} and A_{al-8} cells, are maintained normally (yellow arrowheads; see also supplementary material Fig. S8). Plzf^{neg}/Kit^{pos} spermatogonia are barely detectable in Np95 cKO mice (g,h). In Np95 cKO mice, Np95 expression was undetectable (i), confirming Np95 depletion. L, Leydig cells; DAPI, blue. Scale bars: 100 μm in a,f; 50 μm in b-e,g-j.

Our results show that 2 weeks after the first tamoxifen injection, Np95-deficient mice had significantly smaller testes compared with littermate controls (Fig. 5A,B). Although Np95-deficient and littermate control testes contained a similar proportion of Plzf^{pos} spermatogonia per seminiferous tubule, Np95-deficient testes contained far fewer Kit^{pos} spermatogonia, suggesting Np95 is required for either the Kit^{neg} to Kit^{pos} transition or the maintenance of Kit^{pos} spermatogonia (Fig. 6A-C). Additionally, Np95 cKO testis contained residual spermatogonia that showed weak signals of H3K9me2 modification and 5mC (supplementary material Fig. S7A,B). Np95 cKO testes analyzed by whole-mount immunohistochemical analysis revealed that the residual spermatogonia were primarily made up of single cells, paired cells, and chains of four and (less frequently) eight cells (Fig. 6D; supplementary material Fig. S8A,B). In contrast to controls, 16-cell chains were almost absent in Np95 cKO mouse testes (supplementary material Fig. S8B). To assess the cell-cycle status of these residual spermatogonia, they were stained with Ki67, a proliferation marker (Scholzen and Gerdes, 2000). In testes of 4-week-old Np95 cKO mice, 36% of Plzf^{pos} spermatogonia were Ki67^{pos}, which is similar to the proportion seen in control mice, suggesting that these Np95 cKO spermatogonia were proliferating normally (supplementary material Fig. S9). Thus, the residual spermatogonia are not quiescent, given that spermatogonia from A_s to A_{al} divide at least two or three times over 8.6 days (Tegelenbosch and de Rooij, 1993). To check the effect of Np95 cKO on testicular somatic cells, we analyzed expression of: Gata4 and the cytochrome P450 side chain cleavage enzyme (Cyp450) in Leydig cells; Gata4 in Leydig and Sertoli cells; and Sox9 in Sertoli cells. Expression levels of these were similar in Np95 cKO mice and littermate controls (supplementary material Fig. S10A,B), probably because most somatic cells are post-mitotic (Clermont and Perey, 1957;

Kluin et al., 1984; Levine et al., 2000). Together, these data suggest that the influence of the Np95 cKO is restricted to germ cells in the testis. These results suggest that Np95 is necessary for either Kit^{neg} to Kit^{pos} transition or maintenance of Kit^{pos} spermatogonia.

DISCUSSION

This study characterized a previously unidentified epigenetic shift crucial for spermatogonia to transition from A_{al} (Kit^{neg}) to A_1 (Kit^{pos}). Multiple epigenetic changes arise, including an increase in Dnmt3a2/3b protein expression and changes in chromatin modifications (i.e. increase of 5mC signal, accumulation of the H3K9me2 mark and distribution changes of the H3K9me3 associated with DAPI-dense foci; Fig. 7). Our findings suggest significant epigenetic changes occur at the A_{al} to A_1 transition, a period when spermatogonial nuclear architecture transforms. As this transition reportedly occurs without cell division (de Rooij, 2001; Russell et al., 1999), the changes in gene expression and resulting switches in cell identity might depend on such epigenetic dynamics.

In spermatogonia, disrupting Np95 probably blocks differentiation towards or after the Kit^{pos} transition. Np95 mainly functions to maintain patterns of global DNA methylation; it does this by binding the histone modification H3K9me2/3, and by recruiting Dnmt1, a maintenance methyltransferase (Liu et al., 2013; Nady et al., 2011; Rottach et al., 2010). Therefore, Np95 deficiency might trigger global hypomethylation and loss of association with H3K9me2/3 methylation during the Kit^{neg} to Kit^{pos} transition, and impair spermatogonial differentiation. Nevertheless, Np95 KO testes contain some residual A_s to A_{al} spermatogonia that are Kit^{neg}; these likely contain the stem cell population, and can probably tolerate low levels of cytosine methylation.

Similar effects were reported in pluripotent ES cells. Deficiency in Dnmts and Np95 does not alter the undifferentiated status of these cells, according to the studies using hypomethylated cell lines, namely, double-KO (*Dnmt3a*$^{-/-}$ and *Dnmt3b*$^{-/-}$), triple-KO (*Dnmt3a*$^{-/-}$, *Dnmt3b*$^{-/-}$ and *Dnmt1*$^{-/-}$) and *Np95*$^{-/-}$ ES cells (Jackson et al., 2004; Sharif et al., 2007; Tsumura et al., 2006). Nevertheless, these hypomethylated ES cells cannot differentiate, even if leukemia inhibitory factor (LIF) is withdrawn, suggesting intrinsic cellular mechanisms protected these ES from extrinsic differentiation cues (Jackson et al., 2004). Spermatogonia are constantly moving in seminiferous tubules, in a manner different from other tissue-specific stem cells, which settle in niches (Morrison and Spradling, 2008; Nakagawa et al., 2010; Yoshida et al., 2007). Therefore, despite being constantly exposed to extrinsic signals, maintenance of a unique epigenetic state may prevent spermatogonia from differentiating.

In postnatal male germ cells, expression of Dnmt3 may correlate inversely with the timscale of the stem cell activity level. Although in P0.5 testes, gonocytes express high levels of Dnmt3a2, where stem cell activity is very weak (McLean et al., 2003), Kit^{neg} spermatogonia lose Dnmt3a2 expression by the end of the first postnatal week, strongly correlating with the timing of testicular stem cell emergence (McLean et al., 2003; Ohbo et al., 2003). Then, onset of Dnmt3a2 and also 3b expression in Kit^{pos} spermatogonia correlates with the timing of the loss of stem-cell identity (Ohbo et al., 2003; Shinohara et al., 2000). Our methylation analysis with immunohistochemistry and locus-specific bisulfite sequencing suggests methylation changes are actually accompanied by Dnmt changes. Accordingly, in A_s to A_{al} spermatogonia, Ngn3-driven expression of Flag-Dnmt3b increased Kit expression, possibly via increased methylation at genes including *plzf* and *oct4*. In light of the abnormalities of Np95-depleted spermatogonia, these results suggest the DNA methylation machineries (including Np95-mediated molecular events) regulate the Kit^{neg} to Kit^{pos} transition. At this switching point, spermatogonia might lose their stem cell activity and/or the ability to differentiate. Nevertheless, as with a recent methylome analyses, which expanded immunohistochemistry-based views on global methylation patterns in early embryos (Smith et al., 2012; Smallwood et al., 2011), it is important to note that the accurate picture of methylation changes in spermatogonia remain undetermined; future studies should address this point.

H3K9me2 modification has been suggested to reshape the nuclear architecture in a previous study (Wen et al., 2009). In differentiated ES cells, H3K9me2 modifies large genomic regions, forming domains known as large organized chromatin K9-modifications (LOCKs), structures that are associated with nuclear

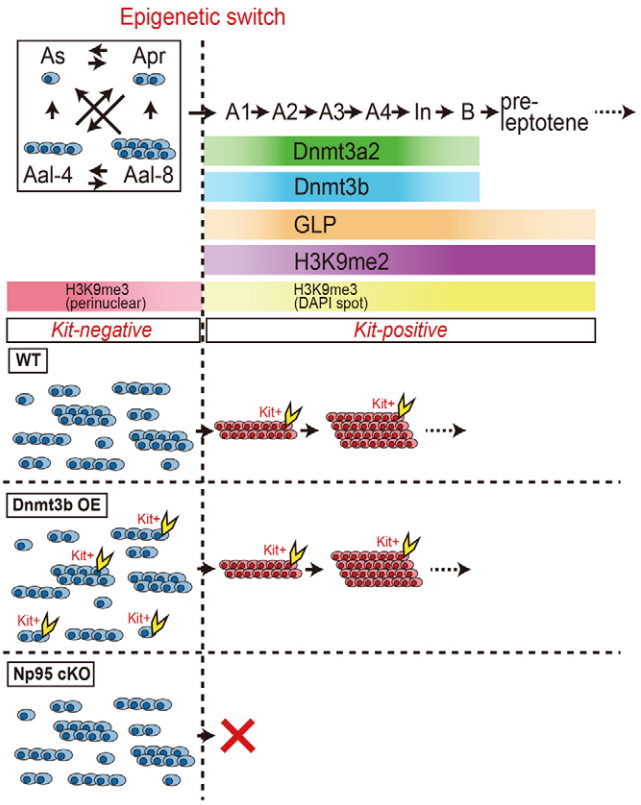

Fig. 7. Model of epigenetic switch during transition from Kit^{neg} to Kit^{pos}. A_s, A_{pr} and A_{al} spermatogonia exhibit similar epigenetic status, showing barely detectable levels of Dnmt3a2/3b and GLP proteins, an absence of H3K9me2 modification, and H3K9me3 localization at the nuclear periphery. These characteristics are indistinguishable, irrespective of marker expression or topological localization of spermatogonia. A_s, A_{pr} and A_{al} spermatogonia are possibly in a 'metastable' state. At the transition from A_{al} to A_1, when cells lose their stem cell activity, they acquire *de novo* DNA methylation, H3K9me2 modification and DAPI-dense foci with translocation of H3K9me3, events that occur simultaneously and without cell division (Russell et al., 1999). Based on mouse knockout phenotypes, failure of Np95-mediated epigenetic events at this transition triggers a differentiation defect. Induction of Dnmt3b alone is enough for induction of the progenitor marker Kit. Theoretically, chromatin reorganization plus two major repressive epigenetic modifications might function as a switching point that governs self-renewal and differentiation.

lamina. Conversely, LOCKs cover little of the genomes of undifferentiated ES cells. This suggests chromosomes assemble nuclear architectures that are differentiation-stage specific (Wen et al., 2009). Thus, as spermatogonia exit from the A_s to A_{al} stages and pass to the A_1 stage, H3K9me2 modifications may reshape chromosome structure.

It is notable that H3K9me2 modification was not elicited by ectopic Dnmt3b expression in testes, although Kit expression was induced. This result suggests the Dnmt3b-mediated DNA methylation pathway does not trigger H3K9me2 accumulation in Kit^{pos} spermatogonia. In addition, knocking out a major mammalian methyltransferase for H3K9me2, G9a, did not affect expression of Dnmt3a2 and Dnmt3b at the Kit^{neg} to Kit^{pos} transition in mouse testis (data not shown); rather, abnormal phenotypes do not arise until the meiotic phase (Tachibana et al., 2007). Nevertheless, as GLP greatly stimulates G9a activity (Tachibana et al., 2005), GLP might trigger genome-wide accumulation of H3K9me2 during Kit^{neg} to Kit^{pos} transition, as GLP becomes upregulated in Kit^{pos} spermatogonia.

How do DNA methylation and histone modifications regulate spermatogonial differentiation? Hypothetically, such epigenetic modifications induce changes in nuclear architecture that globally alter gene expression networks, so particular sets of genes are expected to be targeted by DNA methylation and/or histone modifications. Indeed, we observed methylation changes at the regulatory regions of *plzf* and *oct4*, both of which are used as markers for undifferentiated spermatogonia (Pesce et al., 1998; Buaas et al., 2004; Costoya et al., 2004). Further studies might elucidate the mechanistic link between the epigenetic dynamics and differentiation of spermatogonia on a global scale. In particular, it is important to clarify the genomic targets of *de novo* Dnmts- and H3K9-modified regions, but it will be difficult to carry out these experiments owing to the current technical limitations.

In this study, we observed little epigenetic or phenotypic difference among A_s, A_{pr} and A_{al} cells, regardless of where they localized on the seminiferous epithelium or the types of markers they expressed. This is in contrast to the dramatic differences seen at the A_{al} to A_1 transition. Our finding of the epigenetic uniformity might indicate that A_s to A_{al} spermatogonia form a stem cell pool (Fig. 7). The hypothesis of a stem cell pool is supported by a number of previous reports revealing that A_s to A_{al} cells share many properties: multiple spermatogonial markers are expressed in not only A_s but also A_{pr} and A_{al} cells (Buaas et al., 2004; Costoya et al., 2004; Yoshida et al., 2004; Buageaw et al., 2005; Tokuda et al., 2007; Suzuki et al., 2009; Zheng et al., 2009); A_s, A_{pr} and A_{al} cells are only distinguished by chain length, exhibiting no other morphological differences (Kluin and de Rooij, 1981; de Rooij, 1998; Chiarini-Garcia and Russell, 2001); and mitosis of A_s to A_{al} cells is asynchronous, although spermatogonia differentiating from A_1 cells undergo synchronous divisions (Huckins, 1971; Lok and de Rooij, 1983; Lok et al., 1983; de Rooij, 1998). Evaluation of the stem cell activity of A_{pr} and A_{al} cells is needed because our approach may not be sufficient for detecting early changes that could progressively specify cell fate during divisions that might commence in A_{pr} and A_{al} cells, but it is possible that A_s to A_{al} spermatogonia are epigenetically confined in a stem cell pool until they reach a point of no return. Thus, our analysis of spermatogonia from an epigenetic perspective broadens a marker-based view of the testicular stem cell system, and might provide a novel approach to distinguish stem cells from progenitor cells.

Acknowledgements
We are grateful to Dr Yoshiakira Kanai (Tokyo University) for the Sox9 antibody, to Dr Yoshitake Nishimune (Osaka University) for TRA98 antibody, to Mr Atsushi Tanaka for cell sorting, and to Dr Alexander Brehm, Dr Patrick Varga-weisz, Dr Elise Lamar and Dr Hiroko Iwasaki for critical reading of the manuscript.

Funding
This work is supported by a Grant-in-Aid from the Ministry of Education, Culture, Sports, Science and Technology (MEXT) of Japan for Scientific Research on Innovative Areas on 'Regulatory Mechanism of Gamete Stem Cells' to K.O.

Competing interests statement
The authors declare no competing financial interests.

Author contributions
T.S. designed, performed and analyzed most experiments and wrote the manuscript. R.Y.-D., A.Y., Y.T.-H., K.U. and M.M. prepared and provided materials. S.T. performed immunohistochemical analysis and wrote the manuscript. Y.K., K.N., H.S. and Y.S. performed immunohistochemical analysis. J.S. contributed to methylation analysis. A.Y. contributed to molecular analysis. S.Y. and H.K. provided materials and participated in discussion. T.S. supervised the study and participated in discussion. K.O. designed and supervised the study and wrote the manuscript. All authors were involved in the final stages of writing the article.

Supplementary material
Supplementary material available online at
http://dev.biologists.org/lookup/suppl/doi:10.1242/dev.094045/-/DC1

References
Bártová, E., Krejcí, J., Harnicarová, A., Galiová, G. and Kozubek, S. (2008). Histone modifications and nuclear architecture: a review. *J. Histochem. Cytochem.* **56**, 711-721.
Bostick, M., Kim, J. K., Estève, P. O., Clark, A., Pradhan, S. and Jacobsen, S. E. (2007). UHRF1 plays a role in maintaining DNA methylation in mammalian cells. *Science* **317**, 1760-1764.
Brinster, R. L. (2002). Germline stem cell transplantation and transgenesis. *Science* **296**, 2174-2176.
Buaas, F. W., Kirsh, A. L., Sharma, M., McLean, D. J., Morris, J. L., Griswold, M. D., de Rooij, D. G. and Braun, R. E. (2004). Plzf is required in adult male germ cells for stem cell self-renewal. *Nat. Genet.* **36**, 647-652.
Buageaw, A., Sukhwani, M., Ben-Yehudah, A., Ehmcke, J., Rawe, V. Y., Pholpramool, C., Orwig, K. E. and Schlatt, S. (2005). GDNF family receptor alpha1 phenotype of spermatogonial stem cells in immature mouse testes. *Biol. Reprod.* **73**, 1011-1016.
Chiarini-Garcia, H. and Russell, L. D. (2001). High-resolution light microscopic characterization of mouse spermatogonia. *Biol. Reprod.* **65**, 1170-1178.
Chiarini-Garcia, H. and Russell, L. D. (2002). Characterization of mouse spermatogonia by transmission electron microscopy. *Reproduction* **123**, 567-577.
Clermont, Y. and Perey, B. (1957). Quantitative study of the cell population of the seminiferous tubules in immature rats. *Am. J. Anat.* **100**, 241-267.
Costoya, J. A., Hobbs, R. M., Barna, M., Cattoretti, G., Manova, K., Sukhwani, M., Orwig, K. E., Wolgemuth, D. J. and Pandolfi, P. P. (2004). Essential role of Plzf in maintenance of spermatogonial stem cells. *Nat. Genet.* **36**, 653-659.
Cremer, T. and Cremer, C. (2001). Chromosome territories, nuclear architecture and gene regulation in mammalian cells. *Nat. Rev. Genet.* **2**, 292-301.
de Rooij, D. G. (1998). Stem cells in the testis. *Int. J. Exp. Pathol.* **79**, 67-80.
de Rooij, D. G. (2001). Proliferation and differentiation of spermatogonial stem cells. *Reproduction* **121**, 347-354.
de Rooij, D. G. and Russell, L. D. (2000). All you wanted to know about spermatogonia but were afraid to ask. *J. Androl.* **21**, 776-798.
Filipponi, D., Hobbs, R. M., Ottolenghi, S., Rossi, P., Jannini, E. A., Pandolfi, P. P. and Dolci, S. (2007). Repression of kit expression by Plzf in germ cells. *Mol. Cell. Biol.* **27**, 6770-6781.
Graf, T. and Stadtfeld, M. (2008). Heterogeneity of embryonic and adult stem cells. *Cell Stem Cell* **3**, 480-483.
Grewal, S. I. and Jia, S. (2007). Heterochromatin revisited. *Nat. Rev. Genet.* **8**, 35-46.
Hajkova, P., Jeffries, S. J., Lee, C., Miller, N., Jackson, S. P. and Surani, M. A. (2010). Genome-wide reprogramming in the mouse germ line entails the base excision repair pathway. *Science* **329**, 78-82.
Hirasawa, R., Chiba, H., Kaneda, M., Tajima, S., Li, E., Jaenisch, R. and Sasaki, H. (2008). Maternal and zygotic Dnmt1 are necessary and sufficient for the maintenance of DNA methylation imprints during preimplantation development. *Genes Dev.* **22**, 1607-1616.

Huckins, C. (1971). The spermatogonial stem cell population in adult rats. I. Their morphology, proliferation and maturation. *Anat. Rec.* **169**, 533-557.
Jackson, M., Krassowska, A., Gilbert, N., Chevassut, T., Forrester, L., Ansell, J. and Ramsahoye, B. (2004). Severe global DNA hypomethylation blocks differentiation and induces histone hyperacetylation in embryonic stem cells. *Mol. Cell. Biol.* **24**, 8862-8871.
Jeltsch, A. (2006). Molecular enzymology of mammalian DNA methyltransferases. *Curr. Top. Microbiol. Immunol.* **301**, 203-225.
Kluin, P. M. and de Rooij, D. G. (1981). A comparison between the morphology and cell kinetics of gonocytes and adult type undifferentiated spermatogonia in the mouse. *Int. J. Androl.* **4**, 475-493.
Kluin, P. M., Kramer, M. F. and de Rooij, D. G. (1984). Proliferation of spermatogonia and Sertoli cells in maturing mice. *Anat. Embryol. (Berl.)* **169**, 73-78.
La Salle, S. and Trasler, J. M. (2006). Dynamic expression of DNMT3a and DNMT3b isoforms during male germ cell development in the mouse. *Dev. Biol.* **296**, 71-82.
Levine, E., Cupp, A. S., Miyashiro, L. and Skinner, M. K. (2000). Role of transforming growth factor-alpha and the epidermal growth factor receptor in embryonic rat testis development. *Biol. Reprod.* **62**, 477-490.
Liu, X., Gao, Q., Li, P., Zhao, Q., Zhang, J., Li, J., Koseki, H. and Wong, J. (2013). UHRF1 targets DNMT1 for DNA methylation through cooperative binding of hemi-methylated DNA and methylated H3K9. *Nat. Commun.* **4**, 1563.
Lok, D. and de Rooij, D. G. (1983). Spermatogonial multiplication in the Chinese hamster. I. Cell cycle properties and synchronization of differentiating spermatogonia. *Cell Tissue Kinet.* **16**, 7-18.
Lok, D., Jansen, M. T. and de Rooij, D. G. (1983). Spermatogonial multiplication in the Chinese hamster. II. Cell cycle properties of undifferentiated spermatogonia. *Cell Tissue Kinet.* **16**, 19-29.
Loukinov, D. I., Pugacheva, E., Vatolin, S., Pack, S. D., Moon, H., Chernukhin, I., Mannan, P., Larsson, E., Kanduri, C., Vostrov, A. A. et al. (2002). BORIS, a novel male germ-line-specific protein associated with epigenetic reprogramming events, shares the same 11-zinc-finger domain with CTCF, the insulator protein involved in reading imprinting marks in the soma. *Proc. Natl. Acad. Sci. USA* **99**, 6806-6811.
May, G. and Enver, T. (2001). *The Lineage Commitment and Self-Renewal of Blood Stem Cells in Hematopoiesis* (ed. L. I. Zon), pp. 61-81. New York, NY: Oxford University Press.
McLean, D. J., Friel, P. J., Johnston, D. S. and Griswold, M. D. (2003). Characterization of spermatogonial stem cell maturation and differentiation in neonatal mice. *Biol. Reprod.* **69**, 2085-2091.
Meilinger, D., Fellinger, K., Bultmann, S., Rothbauer, U., Bonapace, I. M., Klinkert, W. E., Spada, F. and Leonhardt, H. (2009). Np95 interacts with de novo DNA methyltransferases, Dnmt3a and Dnmt3b, and mediates epigenetic silencing of the viral CMV promoter in embryonic stem cells. *EMBO Rep.* **10**, 1259-1264.
Morrison, S. J. and Spradling, A. C. (2008). Stem cells and niches: mechanisms that promote stem cell maintenance throughout life. *Cell* **132**, 598-611.
Muzumdar, M. D., Tasic, B., Miyamichi, K., Li, L. and Luo, L. (2007). A global double-fluorescent Cre reporter mouse. *Genesis* **45**, 593-605.
Nady, N., Lemak, A., Walker, J. R., Avvakumov, G. V., Kareta, M. S., Achour, M., Xue, S., Duan, S., Allali-Hassani, A., Zuo, X. et al. (2011). Recognition of multivalent histone states associated with heterochromatin by UHRF1 protein. *J. Biol. Chem.* **286**, 24300-24311.
Nakagawa, T., Sharma, M., Nabeshima, Y., Braun, R. E. and Yoshida, S. (2010). Functional hierarchy and reversibility within the murine spermatogenic stem cell compartment. *Science* **328**, 62-67.
Oakberg, E. F. (1971). Spermatogonial stem-cell renewal in the mouse. *Anat. Rec.* **169**, 515-531.
Ohbo, K., Yoshida, S., Ohmura, M., Ohneda, O., Ogawa, T., Tsuchiya, H., Kuwana, T., Kehler, J., Abe, K., Schöler, H. R. et al. (2003). Identification and characterization of stem cells in prepubertal spermatogenesis in mice small star, filled. *Dev. Biol.* **258**, 209-225.
Ohmura, M., Yoshida, S., Ide, Y., Nagamatsu, G., Suda, T. and Ohbo, K. (2004). Spatial analysis of germ stem cell development in Oct-4/EGFP transgenic mice. *Arch. Histol. Cytol.* **67**, 285-296.
Okada, Y., Scott, G., Ray, M. K., Mishina, Y. and Zhang, Y. (2007). Histone demethylase JHDM2A is critical for Tnp1 and Prm1 transcription and spermatogenesis. *Nature* **450**, 119-123.
Papait, R., Pistore, C., Negri, D., Pecoraro, D., Cantarini, L. and Bonapace, I. M. (2007). Np95 is implicated in pericentromeric heterochromatin replication and in major satellite silencing. *Mol. Biol. Cell* **18**, 1098-1106.
Papait, R., Pistore, C., Grazini, U., Babbio, F., Cogliati, S., Pecoraro, D., Brino, L., Morand, A. L., Dechampesme, A. M., Spada, F. et al. (2008). The PHD domain of Np95 (mUHRF1) is involved in large-scale reorganization of pericentromeric heterochromatin. *Mol. Biol. Cell* **19**, 3554-3563.
Payne, C. and Braun, R. E. (2006). Histone lysine trimethylation exhibits a distinct perinuclear distribution in Plzf-expressing spermatogonia. *Dev. Biol.* **293**, 461-472.
Pesce, M., Wang, X., Wolgemuth, D. J. and Schöler, H. (1998). Differential expression of the Oct-4 transcription factor during mouse germ cell differentiation. *Mech. Dev.* **71**, 89-98.
Peters, A. H., O'Carroll, D., Scherthan, H., Mechtler, K., Sauer, S., Schöfer, C., Weipoltshammer, K., Pagani, M., Lachner, M., Kohlmaier, A. et al. (2001). Loss of the Suv39h histone methyltransferases impairs mammalian heterochromatin and genome stability. *Cell* **107**, 323-337.
Phillips, B. T., Gassei, K. and Orwig, K. E. (2010). Spermatogonial stem cell regulation and spermatogenesis. *Philos. Trans. R. Soc. B* **365**, 1663-1678.
Rottach, A., Frauer, C., Pichler, G., Bonapace, I. M., Spada, F. and Leonhardt, H. (2010). The multi-domain protein Np95 connects DNA methylation and histone modification. *Nucleic Acids Res.* **38**, 1796-1804.
Russell, L. D., Ettlin, R. A., Hikim, A. P. S. and Clegg, E. D. (1999). Histological and histopathological evaluation of the testis. In *1. Mammalian Spermatogenesis in Histological and Histopathological Evaluation of the Testis* (ed. L. D. Russel, R. Ettlin, A. P. S. Hikim and E. D. Clegg), pp. 1-40. FL, USA: Cache River Press.
Sada, A., Suzuki, A., Suzuki, H. and Saga, Y. (2009). The RNA-binding protein NANOS2 is required to maintain murine spermatogonial stem cells. *Science* **325**, 1394-1398.
Sakai, Y., Suetake, I., Shinozaki, F., Yamashina, S. and Tajima, S. (2004). Co-expression of de novo DNA methyltransferases Dnmt3a2 and Dnmt3L in gonocytes of mouse embryos. *Gene Expr. Patterns* **5**, 231-237.
Sasaki, H. and Matsui, Y. (2008). Epigenetic events in mammalian germ-cell development: reprogramming and beyond. *Nat. Rev. Genet.* **9**, 129-140.
Scholzen, T. and Gerdes, J. (2000). The Ki-67 protein: from the known and the unknown. *J. Cell. Physiol.* **182**, 311-322.
Schrans-Stassen, B. H., van de Kant, H. J., de Rooij, D. G. and van Pelt, A. M. (1999). Differential expression of c-kit in mouse undifferentiated and differentiating type A spermatogonia. *Endocrinology* **140**, 5894-5900.
Seki, Y., Hayashi, K., Itoh, K., Mizugaki, M., Saitou, M. and Matsui, Y. (2005). Extensive and orderly reprogramming of genome-wide chromatin modifications associated with specification and early development of germ cells in mice. *Dev. Biol.* **278**, 440-458.
Sharif, J., Muto, M., Takebayashi, S., Suetake, I., Iwamatsu, A., Endo, T. A., Shinga, J., Mizutani-Koseki, Y., Toyoda, T., Okamura, K. et al. (2007). The SRA protein Np95 mediates epigenetic inheritance by recruiting Dnmt1 to methylated DNA. *Nature* **450**, 908-912.
Shinohara, T., Orwig, K. E., Avarbock, M. R. and Brinster, R. L. (2000). Spermatogonial stem cell enrichment by multiparameter selection of mouse testis cells. *Proc. Natl. Acad. Sci. USA* **97**, 8346-8351.
Smallwood, S. A., Tomizawa, S., Krueger, F., Ruf, N., Carli, N., Segonds-Pichon, A., Sato, S., Hata, K., Andrews, S. R. and Kelsey, G. (2011). Dynamic CpG island methylation landscape in oocytes and preimplantation embryos. *Nat. Genet.* **43**, 811-814.
Smith, Z. D., Chan, M. M., Mikkelsen, T. S., Gu, H., Gnirke, A., Regev, A. and Meissner, A. (2012). A unique regulatory phase of DNA methylation in the early mammalian embryo. *Nature* **484**, 339-344.
Spangrude, G. J., Heimfeld, S. and Weissman, I. L. (1988). Purification and characterization of mouse hematopoietic stem cells. *Science* **241**, 58-62.
Spinello, I., Quaranta, M. T., Pasquini, L., Pelosi, E., Petrucci, E., Pagliuca, A., Castelli, G., Mariani, G., Diverio, D., Foà, R. et al. (2009). PLZF-mediated control on c-kit expression in CD34(+) cells and early erythropoiesis. *Oncogene* **28**, 2276-2288.
Suzuki, H., Sada, A., Yoshida, S. and Saga, Y. (2009). The heterogeneity of spermatogonia is revealed by their topology and expression of marker proteins including the germ cell-specific proteins Nanos2 and Nanos3. *Dev. Biol.* **336**, 222-231.
Tachibana, M., Ueda, J., Fukuda, M., Takeda, N., Ohta, T., Iwanari, H., Sakihama, T., Kodama, T., Hamakubo, T. and Shinkai, Y. (2005). Histone methyltransferases G9a and GLP form heteromeric complexes and are both crucial for methylation of euchromatin at H3-K9. *Genes Dev.* **19**, 815-826.
Tachibana, M., Nozaki, M., Takeda, N. and Shinkai, Y. (2007). Functional dynamics of H3K9 methylation during meiotic prophase progression. *EMBO J.* **26**, 3346-3359.
Takada, Y., Naruse, C., Costa, Y., Shirakawa, T., Tachibana, M., Sharif, J., Kezuka-Shiotani, F., Kakiuchi, D., Masumoto, H., Shinkai, Y. et al. (2011). HP1γ links histone methylation marks to meiotic synapsis in mice. *Development* **138**, 4207-4217.
Tanaka, H., Pereira, L. A. V. D., Nozaki, M., Tsuchida, J., Sawada, K., Mori, H. and Nishimune, Y. (1997). A germ cell-specific nuclear antigen recognized by a monoclonal antibody raised against mouse testicular germ cells. *Int. J. Androl.* **20**, 361-366.
Tegelenbosch, R. A. J. and de Rooij, D. G. (1993). A quantitative study of spermatogonial multiplication and stem cell renewal in the C3H/101 F1 hybrid mouse. *Mutat. Res.* **290**, 193-200.
Tokuda, M., Kadokawa, Y., Kurahashi, H. and Marunouchi, T. (2007). CDH1 is a specific marker for undifferentiated spermatogonia in mouse testes. *Biol. Reprod.* **76**, 130-141.

Tsumura, A., Hayakawa, T., Kumaki, Y., Takebayashi, S., Sakaue, M., Matsuoka, C., Shimotohno, K., Ishikawa, F., Li, E., Ueda, H. R. et al. (2006). Maintenance of self-renewal ability of mouse embryonic stem cells in the absence of DNA methyltransferases Dnmt1, Dnmt3a and Dnmt3b. *Genes Cells* **11**, 805-814.

Uesaka, T., Jain, S., Yonemura, S., Uchiyama, Y., Milbrandt, J. and Enomoto, H. (2007). Conditional ablation of GFRalpha1 in postmigratory enteric neurons triggers unconventional neuronal death in the colon and causes a Hirschsprung's disease phenotype. *Development* **134**, 2171-2181.

Wen, B., Wu, H., Shinkai, Y., Irizarry, R. A. and Feinberg, A. P. (2009). Large histone H3 lysine 9 dimethylated chromatin blocks distinguish differentiated from embryonic stem cells. *Nat. Genet.* **41**, 246-250.

Yoshida, S., Takakura, A., Ohbo, K., Abe, K., Wakabayashi, J., Yamamoto, M., Suda, T. and Nabeshima, Y. (2004). Neurogenin3 delineates the earliest stages of spermatogenesis in the mouse testis. *Dev. Biol.* **269**, 447-458.

Yoshida, S., Sukeno, M., Nakagawa, T., Ohbo, K., Nagamatsu, G., Suda, T. and Nabeshima, Y. (2006). The first round of mouse spermatogenesis is a distinctive program that lacks the self-renewing spermatogonia stage. *Development* **133**, 1495-1505.

Yoshida, S., Sukeno, M. and Nabeshima, Y. (2007). A vasculature-associated niche for undifferentiated spermatogonia in the mouse testis. *Science* **317**, 1722-1726.

Yoshinaga, K., Nishikawa, S., Ogawa, M., Hayashi, S., Kunisada, T., Fujimoto, T. and Nishikawa, S. (1991). Role of c-kit in mouse spermatogenesis: identification of spermatogonia as a specific site of c-kit expression and function. *Development* **113**, 689-699.

Zheng, K., Wu, X., Kaestner, K. H. and Wang, P. J. (2009). The pluripotency factor LIN28 marks undifferentiated spermatogonia in mouse. *BMC Dev. Biol.* **9**, 38.

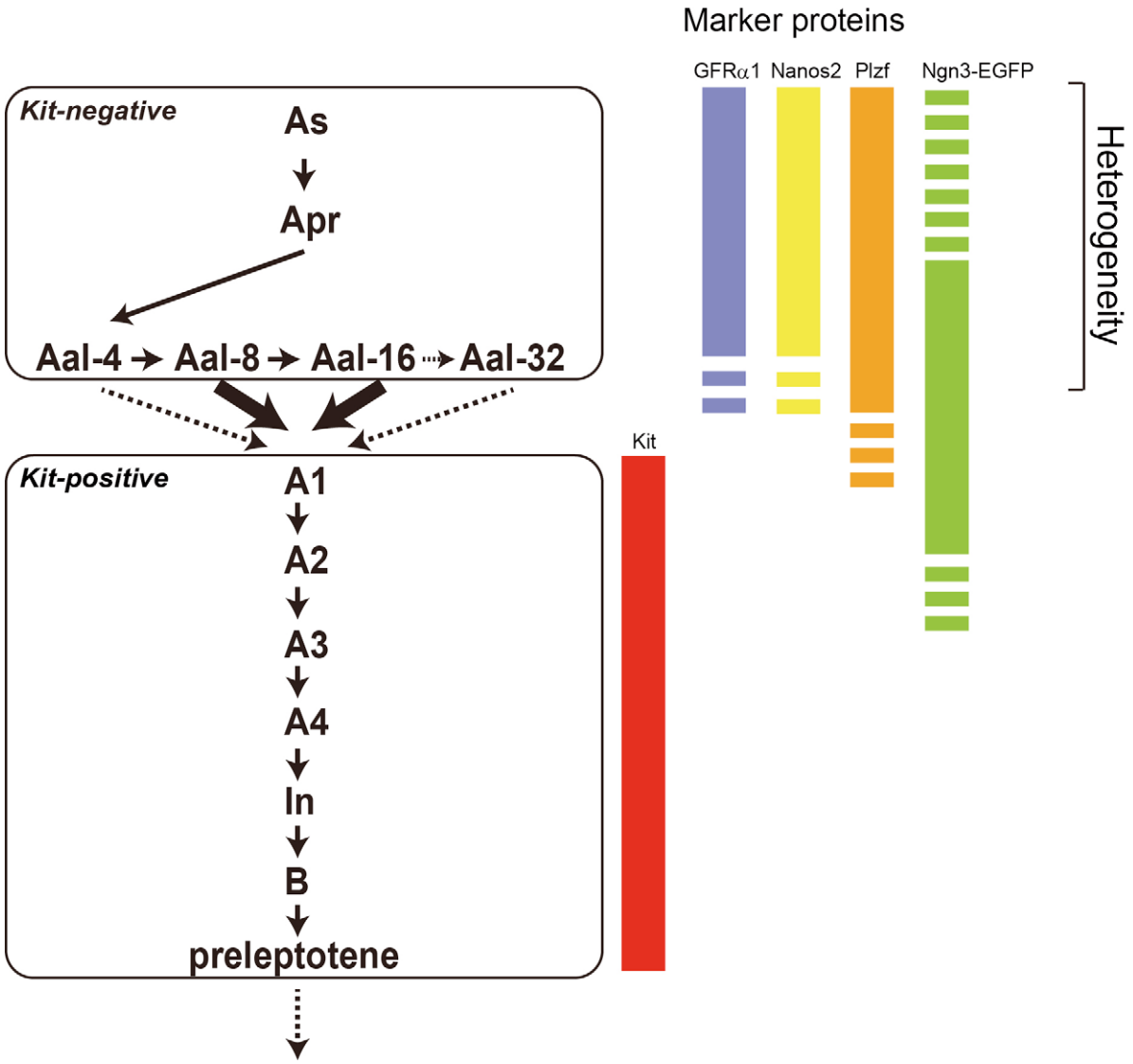

Fig. S1. Schematic representation of spermatogonial differentiation at the adult stage and markers used in this study. Spermatogonial differentiation from Kit^{neg} (A_s-A_{al}) to Kit^{pos} [A_1-A_4, intermediate (In), B] in the adult mouse. Kit expression commences in A_1 cells (Yoshinaga et al., 1991), and is an indicator of differentiated status and loss of stem cell activity (Ohbo et al., 2003; Shinohara et al., 2000). A_1 cells are thought to be the first differentiating spermatogonia, which go through six rounds of synchronous interconnected division (A_1, A_2, A_3, A_4, intermediate and B spermatogonia). GFRα1, Nanos2 and Plzf are expressed mainly in spermatogonia from A_s to A_{al}. In adults, chains of most Ngn3-$EGFP^{pos}$ spermatogonia are longer than those of $GFR\alpha1^{pos}$ and $Nanos2^{pos}$ spermatogonia. Spermatogonial heterogeneity in A_s to A_{al} was revealed by the expression patterns of marker proteins (Suzuki et al., 2007; Nakagawa et al., 2010).

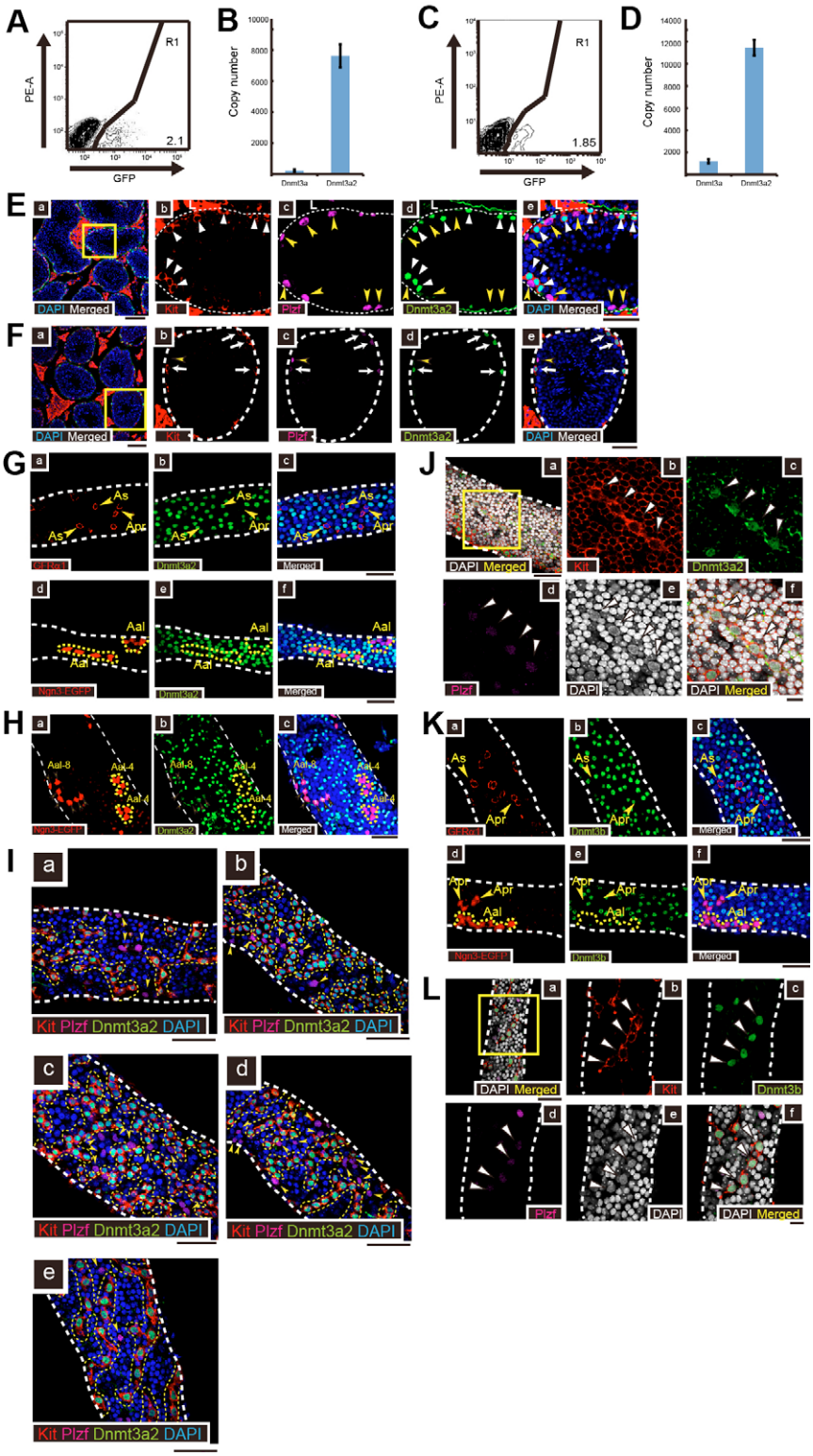

Fig. S2. Dnmt3a2 and Dnmt3b are expressed in Kit^{pos} spermatogonia during neonatal and adult stages. (**A**) Representative FACS plots of P7.5 Oct4-GFP^{pos} mouse testicular cells. Signals from the PE channel served as autofluorescence controls. Dead cells were identified by propidium iodide (PI) staining. GFP^{pos} cells (R1) were sorted and used for qPCR assays. The values presented indicate the percentage of the gated cell population. (**B**) Absolute qPCR using sorted Oct4-GFP^{pos} spermatogonia. Values shown are the mean±s.d. (**C**) Representative FACS plots of 5-week-old Ngn3-EGFP mouse testicular cells. Signals from the PE channel served as autofluorescence controls. Dead cells were eliminated by PI staining. GFP^{pos} cells (R1) were sorted and used for qPCR. The presented numbers denote the percentage of the gated cell population. (**D**) Absolute qPCR using sorted Ngn3-EGFP^{pos} spermatogonia. Values shown are the mean±s.d. (**E**) Immunohistochemical analysis of Dnmt3a2 using adult testis sections. (a) The boxed area is enlarged in b-e. Dnmt3a2 (green) is expressed in Plzf^{heg}/Kit^{pos} (white arrowheads) but not in Plzf^{bos}/Kit^{neg} (yellow arrowheads) spermatogonia. Kit, red. Plzf, magenta. DAPI, blue. L, Leydig cells (Kit^{pos}). Scale bars: 50 μm. (**F**) Immunohistochemical analysis of Dnmt3a2 using adult testis sections. (a) The boxed area is enlarged in b-e. Dnmt3a2 (green) is expressed in Plzf-weak positive/ Kit^{pos} (white arrows) but not in Plzf^{bos}/Kit^{neg} (yellow arrowheads) spermatogonia. Kit, red. Plzf, magenta. DAPI, blue. L, Leydig cells (Kit^{pos}).

Scale bars: 50 μm. (**G**) Whole-mount immunohistochemical analysis of Dnmt3a2 (green) and two stem cell markers (red): GFRα1 (a-c) and Ngn3-GFP (d-f). The white dashed lines outline seminiferous tubules. TOPRO3, blue. (a-c) Wild-type mice. (d-f) Ngn3-GFP mice. Scale bars: 50 μm. (**H**) A subset of $A_{al\text{-}8}$ Ngn3-EGFP^{pos} spermatogonia shows weak Dnmt3a2 expression. Whole-mount immunohistochemical analysis of Ngn3-EGFP mouse testis for Dnmt3a2 and EGFP revealed that Dnmt3a2 is weakly expressed in $A_{al\text{-}8}$ spermatogonia (yellow arrowheads), whereas $A_{al\text{-}4}$ spermatogonia (solid yellow dotted line) do not express Dnmt3a2. White dashed lines outline seminiferous tubules. EGFP, red; Dnmt3a2, green; TOPRO3, blue. Scale bar: 50μm. (**I**) Five representative images of Plzf^{heg}/Kit^{pos} spermatogonia longer than eight chains of cysts (a-e). Yellow dashed lines indicate Plzf^{heg}/Kit^{pos} spermatogonia longer than eight chains of cysts, which are Dnmt3a2^{pos}. Plzf^{pos}/Kit^{neg} spermatogonia lack Dnmt3a2 expression (yellow arrowheads). Dnmt3a2 (green), Plzf (magenta), Kit (red) and DAPI (blue). The white dashed lines outline seminiferous tubules. Scale bars: 50 μm. (**J**) A subpopulation of chains of four Plzf-weak positive/Kit^{pos} spermatogonia at stages VIII-IX expressed Dnmt3a2. The boxed area in a is enlarged in b-f. Kit, red; Dnmt3a2, green; Plzf, magenta; DAPI, gray. Scale bars: 50 μm in a; 10 μm in f. (**K**) Whole-mount immunohistochemical analysis of Dnmt3b (green) and two stem cell markers (red): GFRα1 (a-c) and Ngn3-GFP (d-f). The white dashed lines outline seminiferous tubules. TOPRO3, blue. (a-f) Wild-type mice. (g-i) Ngn3-GFP mice. Scale bars: 50 μm. (**L**) A subpopulation of chains of four Plzf-weak positive/Kit^{pos} spermatogonia at stages VIII-IX expressed Dnmt3b. The boxed area in a is enlarged in b-f. Kit, red; Dnmt3b, green; Plzf, magenta; DAPI, gray. Scale bars: 50 μm in a; 10 μm in f.

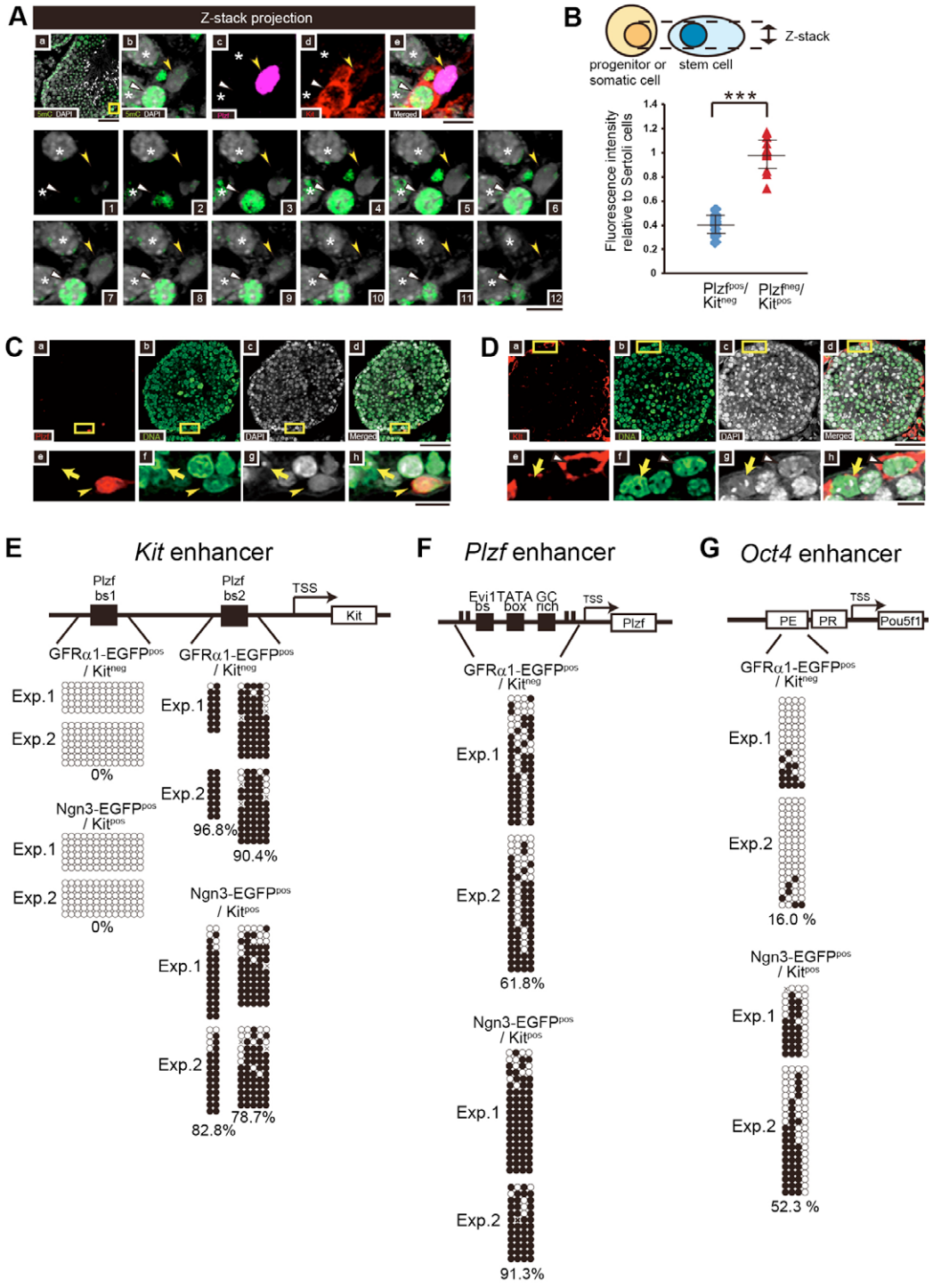

Fig. S3. Immunohistochemical analysis of global DNA methylation and bisulfite sequencing analysis of marker genes for spermatogonia. (**A**) *Z*-stack projection of confocal images (a-e) of Plzf^{pos}/Kit^{neg} and Plzf^{neg} /Kit^{pos} spermatogonia stained with the anti-5mC antibody. Boxed area (a) is enlarged in b-e. Plzf^{pos}/Kit^{neg} spermatogonia (yellow arrowheads) show lower global 5mC levels than Plzf^{neg}/Kit^{pos} spermatogonia (white arrowheads). A *z*-series of twelve confocal images is shown in 1-12. Plzf, magenta; Kit, red; 5mC, green; DAPI, gray. Asterisks indicate spermatocytes. Scale bars: 50 μm in a; 10 μm in e and 12. (**B**) Diagram of *z*-stack confocal analysis. Nuclei from the top to the bottom of spermatogonia and somatic cells were stacked and evaluated for signal strength using NIH Image. Quantification of 5mC signal strength shown as a ratio of 5mC signals from Plzf^{pos}/Kit^{neg} and Plzf^{neg} /Kit^{pos} spermatogonia relative to those of Sertoli cells. *P* values are derived from *t*-tests; ***$P<0.001$. Values shown are mean±s.d. (**C**,**D**) Accessibility of an antibody to genomic DNA under denatured conditions is similar between Plzf^{pos} and Kit^{pos} spermatogonia. Immunohisochemical analysis under denatured conditions using anti-DNA antibody (green) plus anti-Plzf (red in C, yellow arrowheads) or anti-Kit (red in D, white arrowheads) indicates similarly stained nuclei in both cell types. Yellow arrows indicate Sertoli cells. Boxed areas (a-d) are enlarged in e-h. Scale bars: 50 μm in d; 10 μm in h. (**E-G**) Methylation status of *kit* enhancer (E), *plzf* enhancer (F) and *oct4* enhancer (G) in GFRα1-EGFP^{pos}/Kit^{neg} and Ngn3-EGFP^{pos}/Kit^{pos} spermatogonia. Open and filled circles represent unmethylated and methylated cytosines, respectively. Each row of circles represents one bisulfite-sequenced clone. Results of two independent experiments for each region are shown.

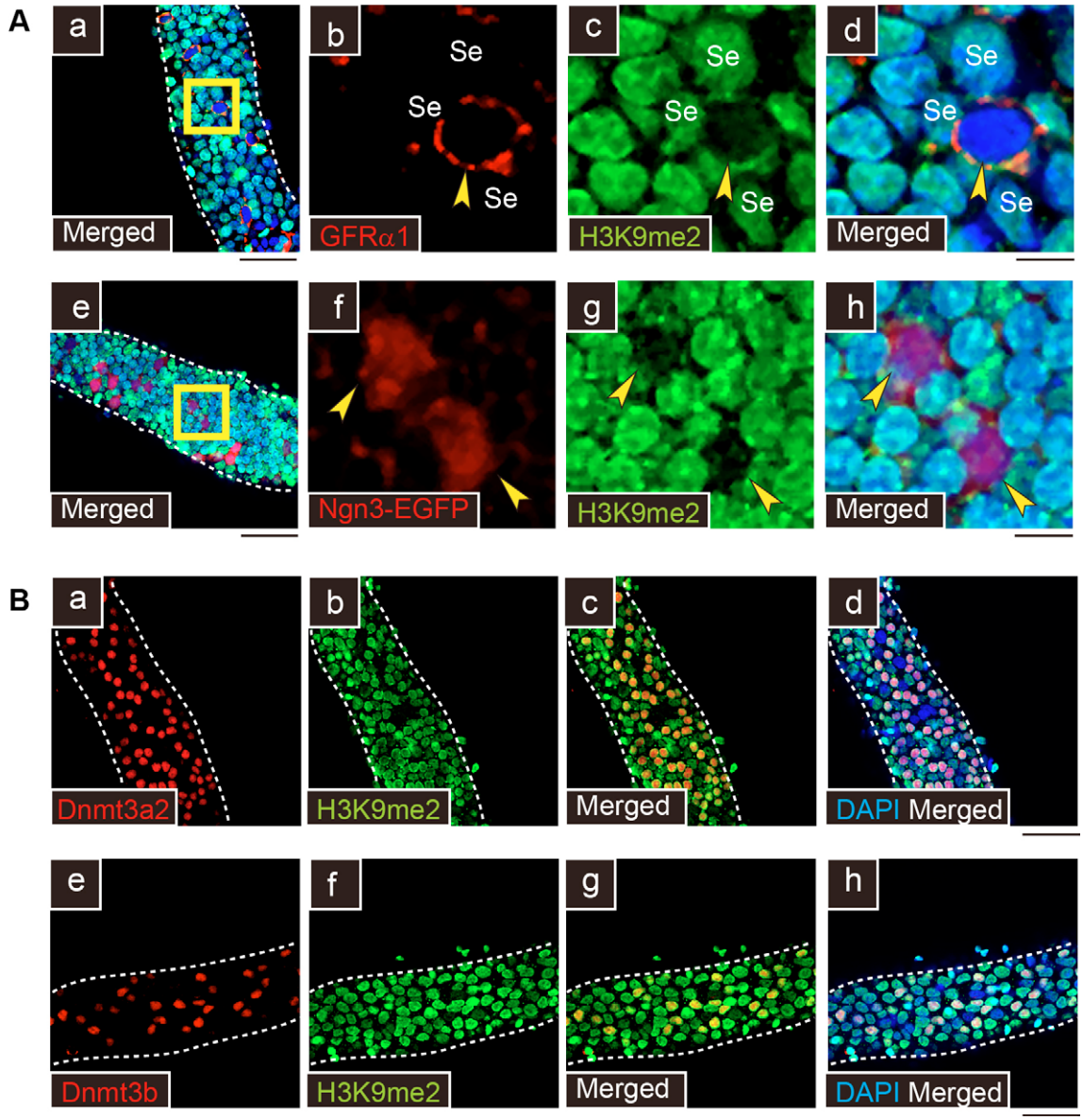

Fig. S4. Concomitant increase in H3K9me2 modification and expression of Dnmt3a2 and Dnmt3b in spermatogonia. (**A**) Spermatogonia expressing GFR 1 (yellow arrowheads) (a-d) and Ngn3-EGFP (yellow arrowheads) (e-h) lack H3K9me2 modification (yellow arrowheads). The boxed areas in a and e are enlarged in b-d and f-h, respectively. Dashed lines outline seminiferous tubules. Se, Sertoli cells. DAPI, blue. Sertoli cells were identified by the pattern of DAPI staining. Scale bars: 50 μm in a,e; 10 μm in d,h. (**B**) Whole-mount immunohistochemical analysis of H3K9me2 (green) co-stained with anti-Dnmt3a2 (red; a,c,d) and anti-Dnmt3b (red; e,g,h) antibodies in wild-type mouse seminiferous tubules. Dnmt3a2^{pos} and Dnmt3b^{pos} spermatogonia are also positive for H3K9me2. Dashed lines outline seminiferous tubules. DAPI, blue. Scale bars: 50 μm.

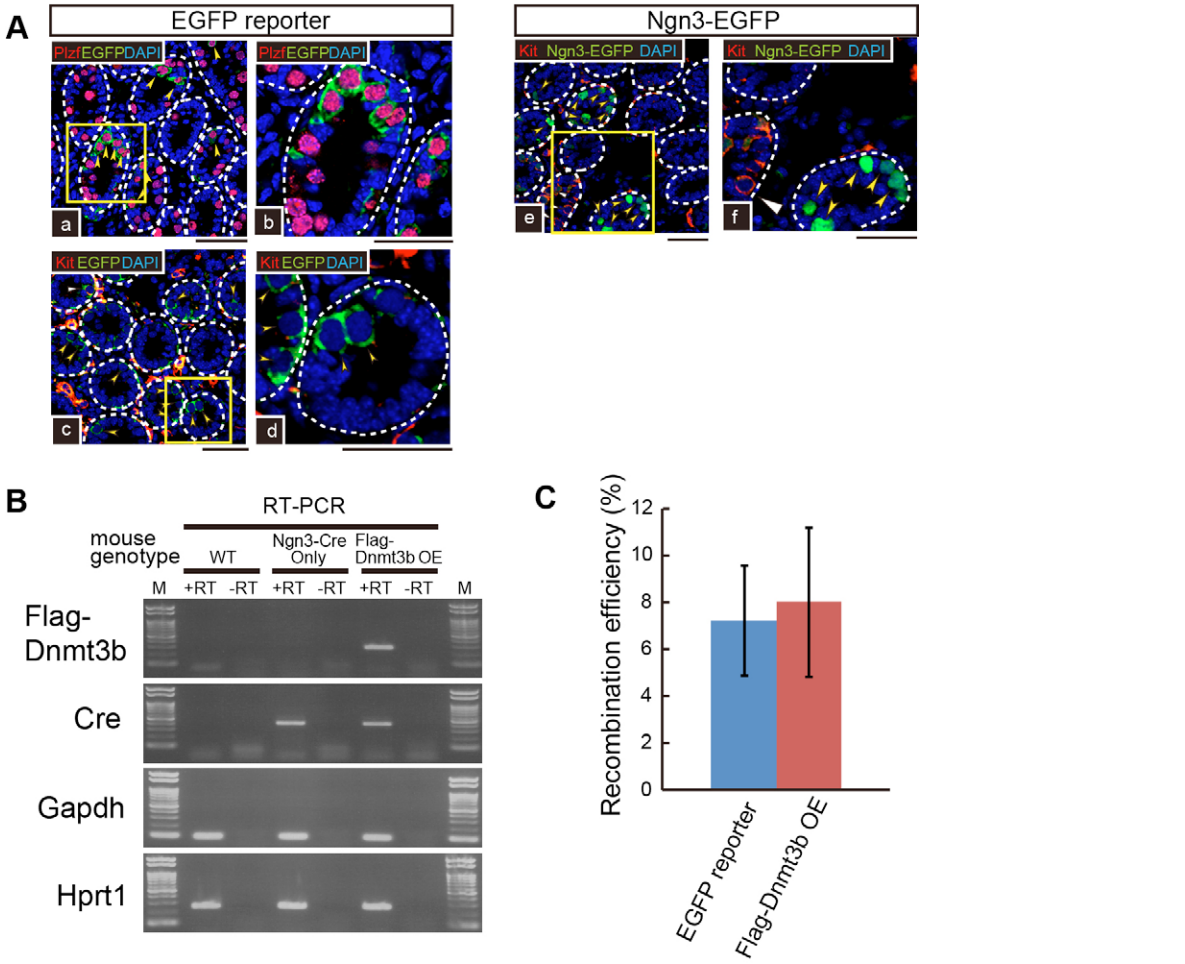

Fig. S5. Confirmation of Flag-Dnmt3b expression and Cre recombination frequency. (**A**) All EGFP-expressing spermatogonia (yellow arrowheads) are Plzf^{pos} at neonatal stages (a-d). Plzf, red; EGFP, green; TOPRO3, blue. Scale bars: 50 μm. White dashed lines outline seminiferous tubules. Most spermatogonia recombined by Ngn3-Cre at P6.5 are Kit negative (c,d). In addition, Ngn3-EGFP^{pos} spermatogonia at P6.5 are mostly Kit negative (e,f). Kit, red; EGFP, green; DAPI, blue. Scale bars: 50 μm. White dashed lines outline seminiferous tubules. (**B**) Efficient transgene excision by Ngn3-cre. RT-PCR analysis of Cre and Flag-Dnmt3b in P6.5 testes with or without reverse transcriptase. M, molecular weight. Only the mice carrying Ngn3-cre:CAG-DsRed-Flag-Dnmt3b transgenes (Flag-Dnmt3b OE mice) expressed Flag-Dnmt3b. (**C**) Comparison of recombination frequency in control EGFP reporter mice and Flag-Dnmt3b OE mice at P6.5. The proportion of EGFP^{pos} cells to TRA98^{pos} cells (blue column) in EGFP reporter mice, and Flag-Dnmt3b^{pos} cells to TRA98^{pos} cells (red column) in Flag-Dnmt3b OE mice was very similar (7±2% and 8±3%, respectively). TRA98 is a germ cell marker (Tanaka et al., 1997). Values are presented as mean±s.d.

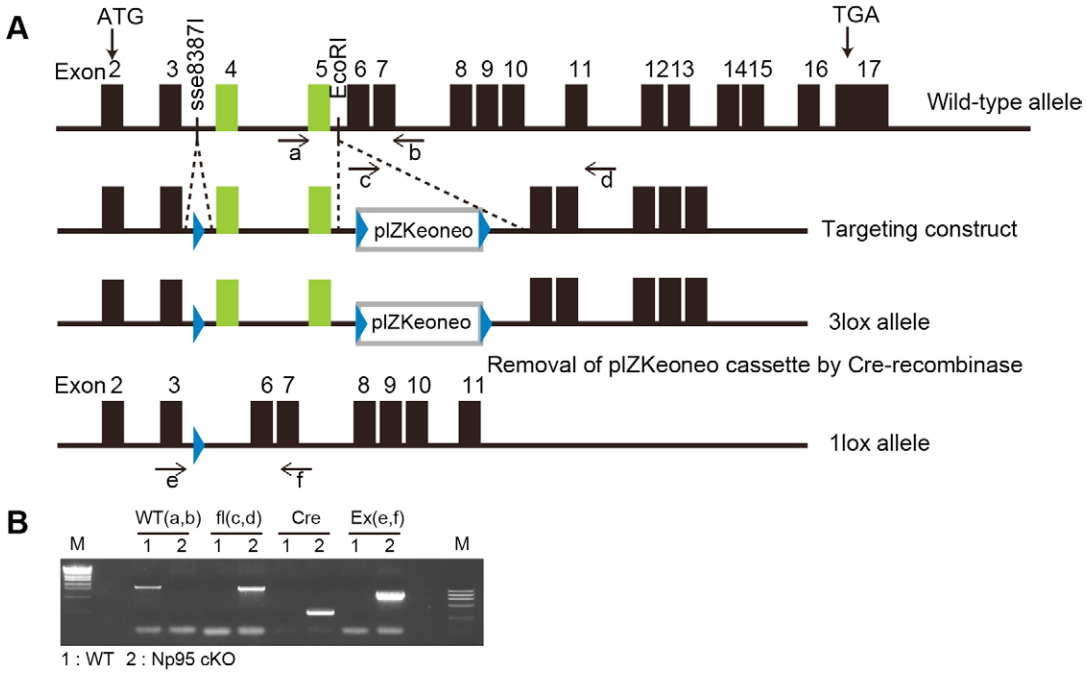

Fig. S6. Generation of Np95 cKO mice. (**A**) Strategy for conditional mutagenesis, and positions of primers for genotyping. (**B**) Confirmation of deletion of the Np95 allele by genomic PCR after tamoxifen treatment. Primers a and b amplify the wild-type allele (WT, 1569 bp), whereas primers c and d detect the floxed allele (fl, 1472 bp). After deletion, primers e and f were used to amplify the deleted allele (Ex, 1006 bp) but the floxed allele is not amplifiable with these primers owing to the extended length. Cre, $CreER^{T2}$ (762 bp). Lane 1, wild-type mice; lane 2, Np95 cKO mice. The positions of primers are shown in A.

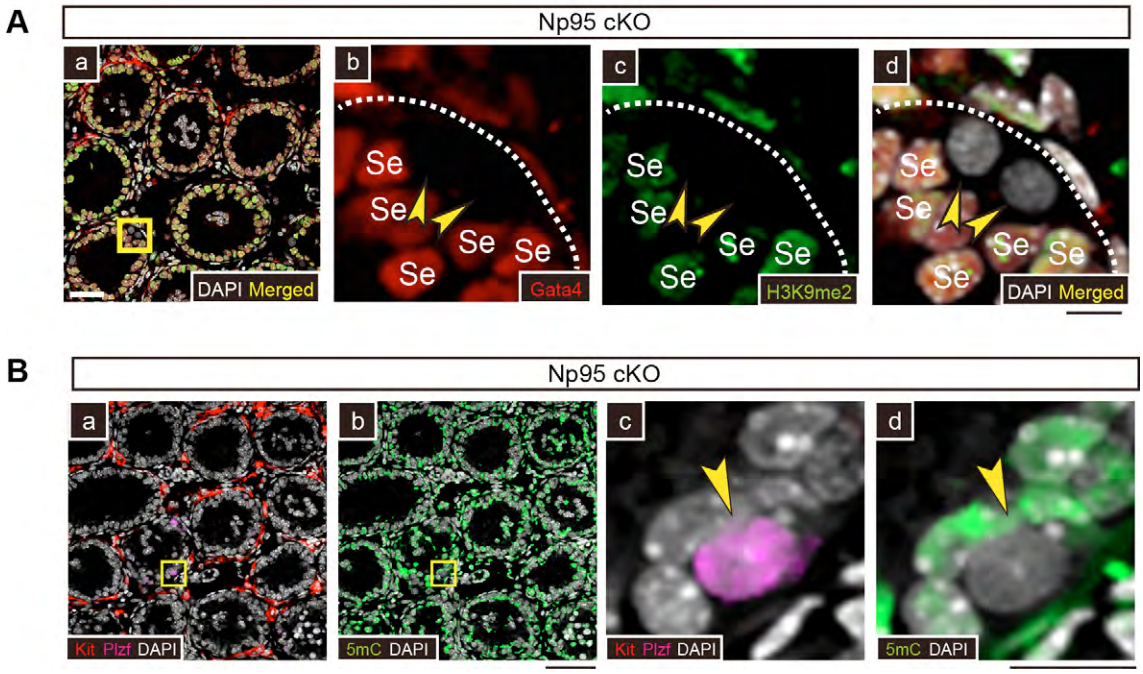

Fig. S7. Spermatogonia in Np95 cKO mouse testis lack H3K9me2 modification and show weak 5mC signals. (**A**) Spermatogonia (yellow arrow) do not exhibit H3K9me2 signals (green) in Np95 cKO mouse testis. $Gata4^{pos}$ Sertoli cells (red, Se) show signs of H3K9me2 modification. Broken white lines outline seminiferous tubules. DAPI, gray. Scale bars: 50 µm (a, white) or 10 µm (d, black). (**B**) Confocal images of Np95 cKO spermatogonia stained with the anti-5mC antibody. Boxed areas (a,b) are enlarged in c,d. Plzf, magenta; Kit, red; 5mC, green and DAPI, gray. Scale bars: 50 µm in b; 10 µm in d.

A

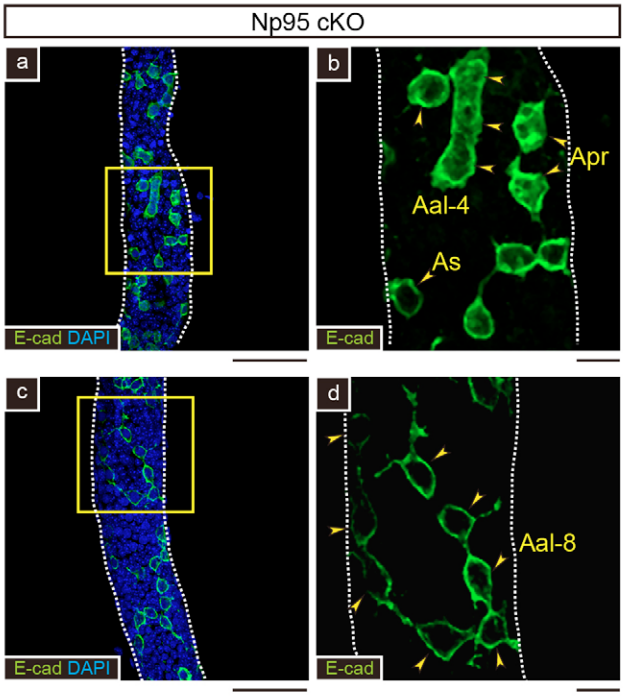

B

number of Ecad^{pos} chained cell	1	2	4	8	more	total
Control	83	79	71	60	102	495
Np95 cKO	72	75	69	15	1	232

Fig. S8. Residual spermatogonia in Np95 cKO mice were primarily made up of single cells, paired cells, and chains of four cells and eight cells. (**A**) Majority of the residual spermatogonia in Np95 cKO mice are A_s, A_{pr}, A_{al-4} or A_{al-8}. Chained spermatogonia were visualized by E-cadherin (green) staining. Boxed areas in a and c are enlarged in b and d, respectively. DAPI, blue. Scale bars: 50 μm in a, c; 10 μm in b,d. (**B**) The number of Ecad^{pos} chained cells in control and Np95 cKO mice was counted to compare the distribution of chain length.

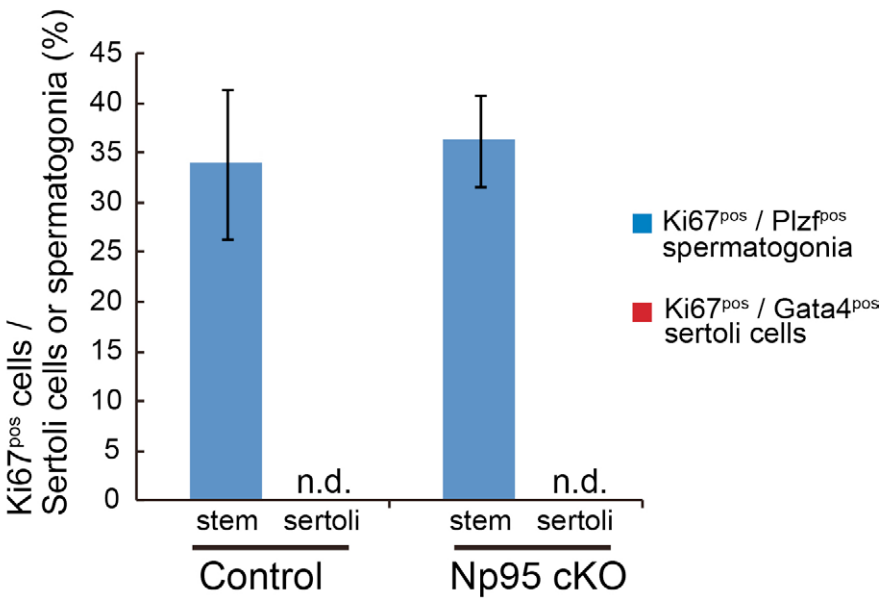

Fig. S9. Cell cycle analysis of Plzf^{pos} spermatogonia in Np95 cKO mice. Cell cycle analysis of Plzf^{pos} spermatogonia and Sertoli cells in Np95 cKO or control mouse testes. The frequency of Ki67^{pos} cells in Plzf^{pos} spermatogonia in 4-week-old Np95 cKO mice was 36%, similar to that seen in littermate control mice. No Ki67^{pos} cells were detected among Gata4^{pos} Sertoli cells in control or Np95 cKO mice. Values are presented as the mean±s.d.

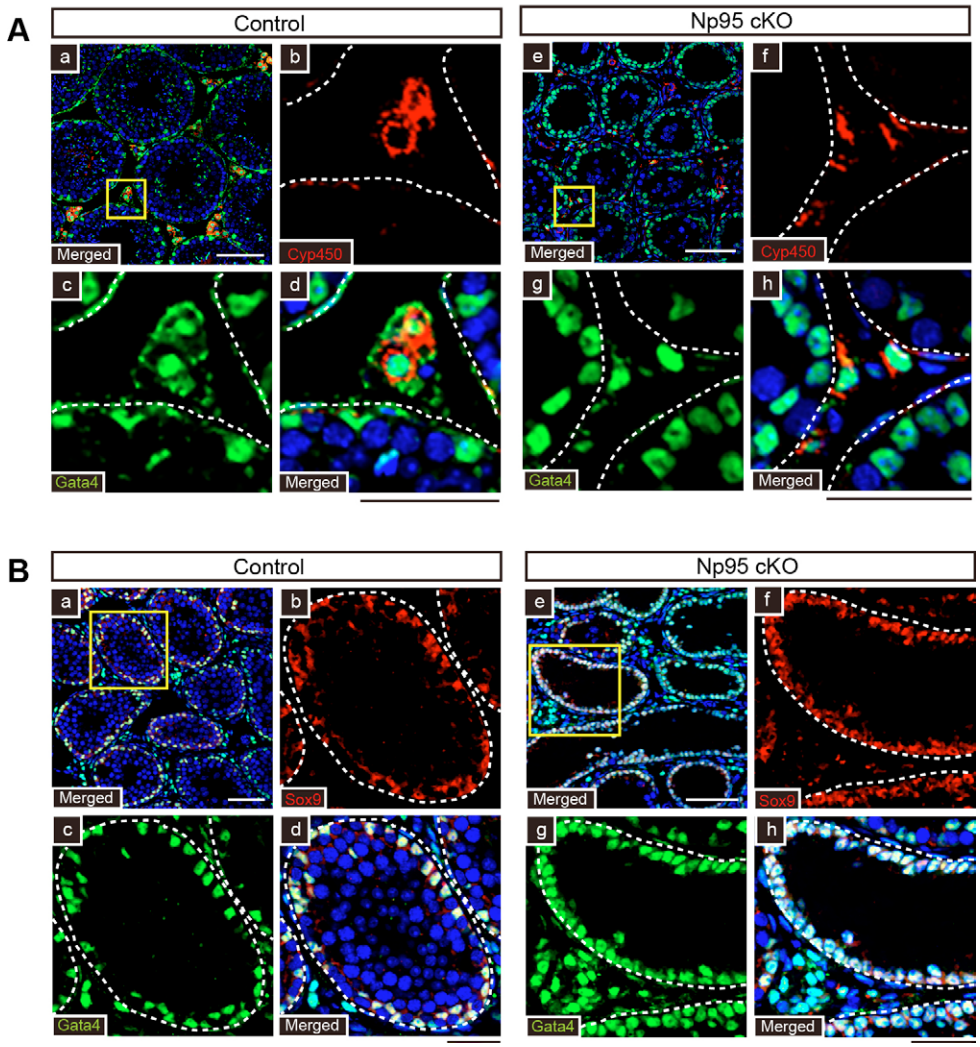

Fig. S10. Analysis of residual somatic cells in Np95 cKO mouse testis. (**A**) Leydig cells express Leydig-specific markers in Np95 cKO mouse testes. The expression level and pattern of Cyp450 (red) and Gata4 (green) were similar between littermate controls (left panels) and Np95 cKO (right panels). Gata4 is also expressed in Sertoli cells. The boxed areas in a and e are enlarged in b-d and f-h, respectively. DAPI, blue. Scale bars: 100 μm (white); 50 μm (black). (**B**) Sertoli cells express Sertoli-specific markers in Np95 cKO mice testes. The expression level and pattern of Sox9 (red) and Gata4 (green) were similar between littermate controls (left panel) and Np95 cKO (right panel). The boxed areas in a and e are enlarged in b-d and f-h, respectively. DAPI, blue. Scale bars: 100 μm (white); 50 μm (black).

Table S1. Primers used in this study

	Forward primer	Reverse primer
Absolute qPCR		
Dnmt3a1	CGACCCATGCCAAGACTCACCTTCCAG	AGACTCTCCAGAGGCCTGGT
Dnmt3a2	CCAGACGGGCAGCTATTTAC	AGACTCTCCAGAGGCCTGGT
RT-PCR		
Flag-*Dnmt3b*	CAAAGACGATGACGACAAGC	CTGTCATGTCCTGCGTGTAA
Cre	GACCATGTCCAATTTACTGACCGTACAC	TTTTGCAGGTTCACCGGCATCAACG
Gapdh	CAATGTGTCCGTCGTGGATCT	GCCTGCTTCACCACCTTCTT
Hprt1	GCTGGTGAAAAGGACCTCT	CACAGGACTAGAACACCTGC
Genotyping		
Np95 cKO WT	GGCCCCTGCCCTTATGGCTTTGCTGGACTCT	GGGGCTGAGCCTGGGCTTCTTCACCCAGGTTGA
Np95 cKO Fl	GCCGGGGCAGGATCTCCTGTCATCTCAC	GGGGCTGCAACAGGCCACCATGCCACCTGGCATTG
Np95 cKO Ex	GCGCCAGAGTCTGGCACTGCCTCTCAGTAC	GCCCACCACACACATGGCAGGCACACT
Np95 cKO CreER^{T2}	GCCTGCATTACCGGTCGATGCAACGA	GTGGCAGATGGCGCGGCAACACCATT
Flag-*Dnmt3b* OE	ACCAGAGGCCGCAGGTCAAGC	CCACTGTACCCAGCGCATTCC
EGFP reporter	TACGGCAAGCTGACCCTGAA	TGTGATCGCGCTTCTCGTTG
Ngn3-Cre	GACCATGTCCAATTTACTGACCGTACAC	TTTTGCAGGTTCACCGGCATCAACG
Bisulfite sequencing		
Kit enhancer Plzf bs1	GTTTACGTGGTTTTTTTTTTTTATTGGGAG	TCCTAACGAACCTTTAATACTACC
Kit enhancer Plzf bs2-1	GTTTATATTTTTAAGTATTTTGTAGGGTTG	AAATTCTTTAAATCCCAAAATTATACAC
Kit enhancer Plzf bs2-2	GGGATTTAAAGAATTTTTAAAATAAA	CCCAAATACTAAAATTAAAATCATAC
Plzf enhancer	ATTGGTTTTTGTTTTTATAGTGTTGG	AAACTCCAAAACATTTCCACTTAAC
Oct4 enhancer	TAAGATGGAATATTGTGTTTTGAAAA	TCAACCATCCTCTAAAAAACCTAAA